

A subseasonal Earth system prediction framework with CESM2

Jadwiga H. Richter¹, Anne A. Glanville¹, James Edwards¹, Brian Kauffman¹, Nicholas A. Lewis², Abigail Jaye³, Hyemi Kim⁴, Nicholas M. Pedatella⁵, Lantao Sun⁶, Judith Berner^{3,1}, Who M. Kim¹, Stephen G. Yeager¹, Gokhan Danabasoglu¹, Julie M. Caron¹, and Keith W. Oleson¹

¹ Climate and Global Dynamics Laboratory, National Center for Atmospheric Research,
Boulder, Colorado

² Atmospheric Chemistry Observations and Modeling Laboratory, National Center for Atmospheric Research, Boulder, Colorado

³ Mesoscale and Microscale Meteorology Laboratory, National Center for Atmospheric Research, Boulder, Colorado

⁴ School of Marine and Atmospheric Sciences, Stony Brook University, Stony Brook, New York

⁵High Altitude Observatory, National Center for Atmospheric Research, Boulder, Colorado

⁶Colorado State University, Fort Collins, Colorado

Key points: (140 char max each)

- A subseasonal research framework with CESM2(CAM6) and CESM2(WACCM6) is described
 - Subseasonal prediction skill of CESM2(CAM6) and CESM2(WACCM6) is similar to that of CESM1(CAM5) and operational models
 - The new framework facilitates predictability research for multiple aspects of the Earth system, including the mesosphere

27 **Abstract**

28 A framework to enable Earth system predictability research on the subseasonal timescale is
29 developed with the Community Earth System Model, version 2 (CESM2) using two model
30 configurations that differ in their atmospheric components. One configuration uses the
31 Community Atmosphere Model, version 6 (CAM6) with its top near 40 km, referred to as
32 CESM2(CAM6). The other employs the Whole Atmosphere Community Climate Model, version
33 6 (WACCM6) whose top extends to \sim 140 km in the vertical and it includes fully interactive
34 tropospheric and stratospheric chemistry (CESM2(WACCM6)). Both configurations were used
35 to carry out subseasonal reforecasts for the time period 1999 to 2020 following the Subseasonal
36 Experiment's (SubX) protocol. CESM2(CAM6) and CESM2(WACCM6) show very similar
37 subseasonal prediction skill of 2-meter temperature, precipitation, the Madden-Julian Oscillation
38 (MJO), and North Atlantic Oscillation (NAO) to the Community Earth System Model, version 1
39 with the Community Atmosphere Model, version 5 (CESM1(CAM5)) and to operational models.
40 CESM2(CAM6) and CESM2(WACCM6) reforecast sets provide a comprehensive dataset for
41 predictability research of multiple Earth system components, including three-dimensional output
42 for many variables, and output specific to the mesosphere and lower-thermosphere (MLT)
43 region. We show that MLT variability can be predicted \sim 10 days in advance of sudden
44 stratospheric warming events. Weekly real-time forecasts with CESM2(WACCM6) contribute to
45 the multi-model mean ensemble forecast used to issue the NOAA weeks 3-4 outlooks. As a
46 freely available community model, both CESM2 configurations can be used to carry out
47 additional experiments to elucidate sources of subseasonal predictability.

48

49 **Plain Language Summary**

50 Sources of subseasonal (i.e., timescale of three to four weeks) predictability for surface
51 temperature, precipitation, and extreme events associated with subseasonal modes of variability
52 are not well understood. In addition, there has been little exploration of the predictability of land,
53 sea-ice, the stratosphere, and the mesosphere lower-thermosphere region. We describe here a
54 subseasonal prediction research framework based on two configurations of the Community Earth
55 System Model, version 2 (CESM2) that differ in their atmospheric components. Both
56 configurations demonstrate subseasonal prediction skill comparable to that of operational
57 models. Reforecasts carried out with two configurations of CESM2 provide a comprehensive
58 dataset for predictability research of multiple aspects of the Earth system, including the
59 mesosphere and lower thermosphere region. Real-time forecasts with these models contribute to
60 the multi-model mean ensemble forecast used to issue the National Oceanic and Atmospheric
61 Administration (NOAA) weeks 3-4 outlooks.

62
63

64 **1 Introduction**

65
66 Interest and demand for skillful subseasonal predictions (i.e., targeting three to four
67 weeks) of the Earth system has grown in the recent decade. Multiple economic sectors such as
68 agriculture, energy, and water management could benefit from improved subseasonal predictions
69 (White et al. 2017). Such a need is a strong motivator of research of sources and limits of
70 subseasonal predictability, including identifying windows of opportunity for increased forecast
71 skill (Mariotti et al., 2020; NAS 2016). The international subseasonal-to seasonal (S2S) project
72 and database (Vitart et al., 2017; Vitart and Robinson 2018) and the National Oceanic and
73 Atmospheric Administration (NOAA) SubX project (Pegion et al., 2019) have been instrumental
74 in providing real-time forecasts and reforecasts (forecasts initialized during the historical period)

75 carried out with multiple operational and research models that serve as a community basis for
76 research on predictability on S2S timescales.

77 Subseasonal prediction research has been focused mostly on prediction of the lowermost
78 atmosphere, in particular surface temperature and precipitation, and extreme events associated
79 with these, such as heat waves, droughts, heavy rainfall and cold outbreaks (Ford et al., 2018; de
80 Andrade et al., 2019; Xiang et al., 2020). Substantial effort has also been invested in assessing
81 predictability of dominant modes of variability on the subseasonal timescale, such as the Madden
82 Julian Oscillation (MJO) and the North Atlantic Oscillation (NAO) as these can be drivers for
83 extreme weather (e.g., Stan et al. 2017; Vitart et al., 2017; Kim et al., 2018; Lim et al., 2018; Sun
84 et al., 2020; Yamagami & Matsueda, 2020). A few recent studies have started examining the
85 predictability of sea-ice and noted a wide range of sea-ice prediction skill, with a multimodel
86 mean forecast being skillful out to 5 months (Wayand et al., 2019; Zampieri et al., 2018). There
87 has also been some exploration of the subseasonal predictability of various land model variables,
88 such as soil moisture and snowpack (Hanchen et al., 2019; Diro & Lin, 2020), however
89 predictability of other characteristics of land has not been explored. Several studies have looked
90 at the predictability of the stratosphere, mainly at the predictability of sudden stratospheric
91 warmings (SSWs), as they can significantly impact surface extreme weather especially over
92 Eurasia (Tripathi et al., 2015), and the predictability of the quasi-biennial oscillation (QBO)
93 which impacts the MJO (Lim et al., 2019; Kim et al., 2019a). Furthermore, there have only been
94 limited efforts aimed at addressing the predictability of variability at higher altitudes (i.e.,
95 mesosphere, thermosphere, and ionosphere) as models used in S2S prediction typically do not
96 extend into that region of the atmosphere. These prior studies have been limited as they used
97 short reforecast periods (Wang et al., 2014; Pedatella et al., 2018a; Pedatella et al., 2019).

98 Variability of the mesosphere and lower-thermosphere (MLT) region drives a significant portion
99 of near-Earth space weather, which can cause adverse effects on communications and navigation
100 systems, and understanding the predictability in the MLT is thus an important component of
101 enhancing space weather forecasting (Jackson et al., 2019).

102 Stratosphere-troposphere interactions provide a potential source of predictability on the
103 S2S timescale because of their persistent and slow varying circulation anomalies (NAS, 2016).
104 Increased predictability is believed to primarily come from SSWs which are followed by
105 tropospheric circulation anomalies resembling the negative phase of the NAO. The QBO has
106 been shown to lead to enhanced predictability on seasonal timescales (e.g., Boer & Hamilton,
107 2008; Marshall & Scaife, 2009), and is predictable out to several years ahead (Scaife et al.,
108 2014b). Hence, a model that represents the QBO and SSWs well could potentially have more
109 skill on the subseasonal timescale.

110 Richter et al. (2020) described the utility of the Community Earth System Model, version
111 1, with the Community Atmosphere Model version 5 as its atmospheric component
112 (CESM1(CAM5)), a predecessor of CESM2, as a subseasonal prediction research model and
113 demonstrated that the prediction skill of key surface variables with that model was comparable to
114 the National Center for Environmental Prediction (NCEP) Climate Forecast System, version 2
115 (CFSv2) operational model. Here, we describe a new community resource for research on
116 subseasonal predictability of multiple components of the Earth system: a subseasonal prediction
117 system based on CESM2 with two configurations that differ in their atmospheric components.
118 One configuration uses the Community Atmosphere Model, version 6 (CAM6), referred to as
119 CESM2(CAM6). The other employs the Whole Atmosphere Community Climate Model, version
120 6 (WACCM6), and is referred to as CESM2(WACCM6). CESM2 is the newest version of the

121 NCAR coupled Earth system model used for the Coupled Model Intercomparison Project phase
122 6 (CMIP6) simulations (Danabasoglu et al., 2020). Both configurations of CESM2 include
123 prognostic atmospheric, land, ocean and sea-ice components and resolve the interactions
124 between them. Both configurations of the model include prognostic aerosols and
125 CESM2(WACCM6) also includes fully interactive tropospheric and stratospheric chemistry.
126 CESM2(WACCM6) has a very good representation of SSWs and an internally generated QBO,
127 hence it potentially could be more skillful, especially during SSW events, than models with
128 smaller vertical domains. Another unique aspect of CESM2(WACCM6) is the extension of the
129 model domain into the lower thermosphere, enabling investigations into the predictability at
130 MLT altitudes. SSW events are now recognized to have impacts throughout the whole
131 atmosphere (Baldwin et al., 2020; Pedatella et al., 2018b), including the mesosphere,
132 thermosphere, and ionosphere, where they influence the day-to-day weather of the near-Earth
133 space environment. It is, therefore, important to understand the predictability of the SSW effects
134 in the middle and upper atmosphere.

135 Weekly real-time forecasts are being generated since September 2020 with
136 CESM2(WACCM6) and since April 2021 with CESM2(CAM6), and they contribute to the
137 multi-model mean ensemble used to issue the experimental NOAA weeks 3-4 outlooks. The
138 motivation behind the inclusion of CESM2(WACCM6) into this NOAA Climate Test Bed
139 project is to examine how much improvement in surface prediction skill can be gained from the
140 inclusion of a well-represented stratosphere, especially during the boreal winter, when the
141 impacts of SSWs on the surface climate and impacts of the QBO on the MJO are the largest.

142 We describe here the S2S prediction framework, reforecasts, and near-real time forecasts
143 with CESM2(CAM6) and CESM2(WACCM6) including the extensive output of atmospheric,

144 land, ocean, and sea-ice models, with several key atmospheric variables reaching into the MLT
145 region. CESM2 is a community model and is freely available to the broader community. The
146 reforecast sets described here are designed to serve as a basis for future experiments with
147 CESM2(CAM6) and CESM2(WACCM6) investigating sources of subseasonal predictability.

148

149 **2 Model and System Description**

150

151 **2.1 Model Description**

152 Subseasonal reforecasts and forecasts described here use the default released version of
153 CESM2. CESM2 is an open-source, comprehensive Earth system model designed primarily for
154 the studies of Earth's past, present and future climates. CESM2 includes ocean, atmosphere,
155 land, sea-ice, land-ice, river, and wave model components and is thoroughly documented in
156 Danabasoglu et al. (2020). The standard CESM2 uses a nominal 1° horizontal resolution (1.25°
157 in longitude and 0.9° in latitude in its atmospheric components). CAM6 is the default
158 atmospheric model. It has 32 vertical levels with the model lid near 2 hPa (~ 40 km). CAM6 uses
159 the Zhang and McFarlane (1995) convection parameterization, the Cloud Layers Unified By
160 Binormals (CLUBB; Golaz et al., 2002; Larson, 2017) unified turbulence scheme, and the
161 updated Morrison-Gettelman microphysics scheme (MG2; Gettelman & Morrison, 2015). A
162 form drag parameterization of Beljaars et al. (2004) and an anisotropic gravity wave drag scheme
163 following Scinocca and McFarlane (2000) replace the turbulent mountain stress parameterization
164 that was used in CESM1. The aerosols in CAM6 are represented using the Modal Aerosol Model
165 version 4 (MAM4) as described in Liu et al. (2016).

166 CESM2(WACCM6) uses WACCM6 or the “high-top” version of the atmospheric model,
167 which is documented in detail in Gettelman et al. (2019). WACCM6 has the same horizontal

168 resolution as CAM6, however it has 70 vertical levels with a top near 4.5×10^{-6} hPa (~ 140 km).
169 The representation of atmospheric physics is identical to that in CAM6, with the only exception
170 being the representation of non-orographic gravity waves, which follows Richter et al. (2010)
171 with changes to tunable parameters described in Gettleman et al. (2019). The higher model lid
172 and parameterization of non-orographic gravity waves in WACCM6 allow for a better
173 representation of middle atmospheric dynamics as compared to CAM6 and the simulation of an
174 internally-generated QBO. Another key difference between CAM6 and WACCM6 is in the
175 representation of chemistry. The comprehensive chemistry module in WACCM6 includes
176 interactive tropospheric, stratospheric, and lower thermospheric chemistry (TSMLT) with 228
177 prognostic chemical species, described in detail in Gettleman et al. (2019). Differences in the
178 representation of aerosols and chemistry between CAM6 and WACCM6 do not significantly
179 impact the mean surface and tropospheric climate in historical simulations. However,
180 CESM2(WACCM6) simulations have a more realistic representation of polar climate as
181 compared to CESM2(CAM6) as shown in Gettleman et al. (2019).

182 CESM2(CAM6) and CESM2(WACCM6) use identical ocean, land, sea-ice, land-ice,
183 river-transport, and wave models. The ocean model is based on the Parallel Ocean Program
184 version 2 (POP2; Smith et al., 2010; Danabasoglu et al., 2012), but contains many advances
185 since its version in CESM1. As described in Danabasoglu et al. (2020), these include a new
186 parameterization for mixing effects in estuaries, increased mesoscale eddy (isopycnal)
187 diffusivities at depth, use of prognostic chlorophyll for shortwave absorption, use of salinity-
188 dependent freezing-point together with the sea-ice model, and a new Langmuir mixing
189 parameterization in conjunction with the new wave model component. Several numerical
190 improvements were also implemented as described in Danabasoglu et al. (2020). The horizontal

191 resolution of POP2 is uniform in the zonal direction (1.125°), and varies from 0.64° (occurring in
192 the Northern Hemisphere) to 0.27° at the Equator. In the vertical, there are 60 levels with a
193 uniform resolution of 10 m in the upper 160m. The ocean biogeochemistry is represented using
194 the Marine Biogeochemistry Library (MARBL), essentially an updated implementation of what
195 has been known as the Biochemistry Elemental Cycle (Moore et al., 2002; 2004; 2013). CESM2
196 includes version 3.14 of the NOAA WaveWatch-III ocean surface wave prediction model
197 (Tolman, 2009). CICE version 5.1.2 (CICE5; Hunke et al., 2015) is used to represent sea-ice in
198 CESM2 and uses the same horizontal grid as POP2. The vertical resolution of sea-ice has been
199 enhanced to eight layers, from four in CESM1; the snow model resolves three layers, and the
200 melt pond parameterization has been updated (Hunke et al., 2013).

201 Both CESM2 configurations use the recently developed Community Land Model version
202 5 (CLM5) described in detail in Lawrence et al., (2019). As compared to CLM4, CLM5 includes
203 improvements to soil hydrology, spatially explicit soil depth, dry surface layer control on soil
204 evaporation, updated ground-water scheme, as well as several snow model updates. CLM5
205 includes a global crop model that treats planting, harvest, grain fill, and grain yields for six crop
206 types (Levis et al., 2018), a new fire model (Li et al., 2013; Li & Lawrence, 2017), multiple
207 urban classes and updated urban energy model (Oleson & Feddema, 2019), and improved
208 representation of plant dynamics. The river transport model is the Model for Scale Adaptive
209 River Transport (MOSART; H. Y. Li et al., 2013). The Community Ice Sheet Model Version
210 2.1 (CISM2.1; Lipscomb et al., 2019) is used to represent the ice sheets, although in the
211 configuration of this model ice sheets are assumed to be fixed.

212

213 **2.2 Initialization**

214 S2S reforecasts with CESM2(CAM6) and CESM2(WACCM6) use the same land initial
215 conditions, but differ in atmosphere, ocean, and sea-ice initialization. These differences are due
216 to the different location of the two atmospheric models' lids and also due the inclusion of
217 CESM2(WACCM) forecasts in NOAA's experimental Week 3-4 outlooks since September
218 2020, necessitating real-time forecasting ability with that model and completion of reforecasts
219 with the same model set-up at that time. Initialization procedures for each model component are
220 described below and summarized in Table 1.

221 Land initial conditions for CESM2(CAM6) and CESM2(WACCM6) reforecasts were
222 produced using the stand-alone CLM5. The stand-alone CLM5 simulation employed a setup
223 consisting of biogeochemistry-driven crops and glacial observations. A 700-year spin-up was
224 performed using 6-hourly atmospheric variables (precipitation, temperature, wind speed,
225 shortwave and longwave radiation, etc.) from the NCEP CFSv2 reanalysis (Saha et al. 2014).
226 Near present-day (year 2000) greenhouse gas forcings were used continuously throughout the
227 spin-up, while atmospheric forcings from NCEP CFSv2 were cycled between 1979-1985 until a
228 steady state was achieved (~100 cycles). After soil moisture and temperatures stabilized with
229 respect to the 1979-1985 climate state, the CLM5 continued to be forced with NCEP CFSv2 up
230 through present day (no longer cyclically), and initial condition files were output for use in
231 reforecasts each Monday.

232 CESM2(CAM6) atmosphere was initialized using the NCEP CFSv2 reanalysis
233 interpolated to the CAM6 grid. Initialized fields include the zonal and meridional wind,
234 temperature, specific humidity, surface pressure and surface geopotential. An ensemble is
235 generated using the random field perturbation method at initial time which was shown to be as

236 effective as other more sophisticated methods to generate model spread by Magnusson et al.
237 (2009) and was utilized successfully in S2S reforecasts with CESM1(CAM5) (Richter et al.
238 2020).

239 Ocean and sea-ice initial conditions for CESM2(CAM6) come from a reforecast ocean-
240 sea-ice coupled configuration of CESM2(CAM6) forced with the adjusted Japanese 55-year
241 reanalysis project state fields and fluxes (JRA55-do forcing; Tsujino et al., 2018). We call this
242 JRA55-do forced ocean simulation (JRA55-do FO). This simulation was integrated through five
243 cycles of the 1958 - 2009 forcing, with the last cycle extended through 2019. This procedure
244 follows the protocol for the CMIP6-endorsed Ocean Model Intercomparison Project phase 2
245 (OMIP2; Griffies et al., 2016; Tusjino et al., 2020), and is the same as was done for S2S
246 reforecasts with CESM1(CAM5) (Richter et al., 2020).

247 The initialization of the atmosphere, ocean, and sea-ice in CESM2(WACCM6) is not as
248 straightforward as for CESM2(CAM6) as the model's lid located near ~ 140 km extends above
249 the currently available atmospheric reanalyses and the JRA55-do was only available through
250 2019 with a yearly update frequency in early 2020 (time of model set-up and running of
251 reforecasts), which prohibited its use in near real-time forecasts. To generate realistic initial
252 conditions for the entire atmospheric domain, first a specified dynamics (SD) simulation with
253 fully coupled CESM2(WACCM6) was carried out (WACCM6-SD) in which the atmospheric
254 dynamics were nudged to the NASA Modern-Era Retrospective Analysis for Research and
255 Applications (MERRA-2) (Gelaro et al. 2017) with a 1-hourly nudging timescale from 1999 to
256 2020. 1-hourly nudging ensured that the dynamics in the lower atmosphere are very close to the
257 MERRA-2 reanalysis, which is important for tropospheric subseasonal prediction. The ocean in
258 this WACCM6-SD simulation is initialized from the JRA55-do FO simulation (as done for

259 CESM2) in year 1998, and then it is left to evolve with atmospheric fluxes from the MERRA-2
260 reanalysis for 5 years. In this set-up, the ocean state drifts from the observed state and the
261 JRA55-do simulation, hence every 5 years the ocean in the SD simulation is reinitialized with the
262 ocean state from the JRA55-do forced ocean simulation. Hence ocean reinitialization occurred
263 on January 1 of 1998, 2003, 2008, 2013, and 2018. We have developed the ability to update the
264 JRA55-do in August of 2020, hence a final ocean reinitialization occurred on August 31 of 2020
265 in order to prime the real-time application which began at that time. Daily atmospheric, ocean
266 and sea-ice, initial conditions were output from the WACCM6-SD simulation for use in
267 reforecasts. The random field perturbation method was applied to the atmospheric conditions to
268 generate ensemble spread in the same way as was done in CESM2(CAM6).

269 Figure 1 shows correlation and root-mean-square error (RMSE) maps between the sea
270 surface temperature (SST) in JRA55-do FO (used to initialize CESM2(CAM6) reforecasts) and
271 HadSST observations (Figs. 1a and 1c) and between SSTs in WACCM6-SD (used to initialize
272 CESM2(WACCM6) reforecasts) and HadSST (Figs. 1b and 1d). Over the 1999 - 2019 period,
273 the correlation between JRA55-do FO and WACCM6-SD and observations is close to 1 over the
274 majority of ocean areas, with the exception of reduced values of the correlation coefficient in the
275 Tropics and south of 50°S. The correlation coefficients are lower in those regions in the
276 WACCM6-SD as compared to the JRA55-do FO simulation. The RMSE distribution (Figure
277 1c,d) is also very similar between JRA55-do FO and WACCM6-SD, with the largest RMSE
278 differences between the two simulations in the Tropics. The larger RMSE in WACCM6-SD as
279 compared to the JRA55-do FO could be related to differences in variability in MERRA-2 as
280 compared to JRA55-do. This greater Tropical drift away from the observed SSTs is illustrated
281 clearly in Figure 1e which shows the El Nino Southern Oscillation (ENSO) index in the JRA55-

282 do FO, WA CCM6-SD, and HadISST. JRA55-do follows the observed ENSO index closely,
283 however there are a few instances when the ENSO index in WACCM-SD departs significantly
284 from observations. This includes the period from ~ 2015 to 2016 and 2019 to 2020.

285 For real-time forecasts with CESM2(WACCM6), the same initialization procedure was
286 used as for reforecasts except that the CESM2(WACCM6) run was nudged to the NASA
287 Forward Processing for Instrument Teams (FP-IT) reanalysis instead of MERRA-2, as the FP-IT
288 reanalysis is available in near real-time.

289

290 **2.3 Protocol and output**

291 The S2S reforecasts were carried out following the SubX protocol (Pegion et al. 2019)
292 with weekly initializations every Monday from 1999 to 2020 for CESM2, and for every Monday
293 between September and March for CESM2(WACCM6). An 11-member ensemble was carried
294 out for the CESM2(CAM6) and a 5-member ensemble was carried out for the
295 CESM2(WACCM6) reforecasts. The computational cost of CESM2(WACCM6) is nearly eight
296 times the cost of CESM2(CAM6), hence carrying out more ensemble members and all start dates
297 was computationally prohibitive with CESM2(WACCM6). Near real-time forecasts began with
298 CESM2(WACCM6) in September of 2020, and in April 2021 with CESM2(CAM6), both with a
299 21-member ensemble.

300 The S2S reforecast set with CESM2(CAM6) and CESM2(WACCM6) have extremely
301 comprehensive output for the atmosphere, land, ocean, and sea-ice components of the model to
302 enable studies of predictability of the broader Earth system, including the MLT region. Output is
303 available from the NCAR Climate Data Gateway (see links in Acknowledgements). The
304 complete list of output variables is shown in Tables S1- S7. Because the reforecasts follow the

305 SubX protocol, a portion of the output also follows that protocol, and a number of model native
306 fields are renamed and reformatted to match the SubX priority 1, 2, and 3 (p1, p2, and p3,
307 respectively) variables. In addition to these variables which are all two-dimensional (on a lat/lon
308 grid), more daily averaged variables are saved for every model component. A handful of
309 atmosphere-relevant variables are saved at 6-hourly intervals for applications such as tropical
310 cyclone tracking. In addition, a limited number of 3-dimensional fields is stored at 14 pressure
311 levels for CESM2(CAM6) and at 22 levels for CESM2(WACCM6) (see Table S4 for exact
312 levels). Finally, for CESM2(WACCM6), diurnal and semidiurnal tide coefficients are stored at 8
313 levels at and above 10 hPa, permitting the evaluation of migrating and nonmigrating tides in the
314 MLT. Because CESM2 includes an interactive crop model, the output list for the land model
315 includes variables such as gross and primary production which are very unique to this dataset.

316

317 **3 Results**

318

319 The subseasonal prediction skill of CESM2(CAM6) and CESM2(WACCM6) in the S2S
320 reforecasts is evaluated for key surface variables (temperature, precipitation), dominant
321 subseasonal modes (MJO and NAO) as well as stratosphere-troposphere coupling. Subsequently
322 we briefly examine MLT predictability during SSWs in CESM2(WACCM6). We compare the
323 tropospheric prediction skill to that from reforecasts carried out with the default version of
324 CESM1(CAM5) utilizing the 30-level version of CAM5 (Richter et al. 2020) for the common
325 period of 1999 to 2015. As the reforecasts with the default (30-level) version of CESM1(CAM5)
326 used a 10-member ensemble, we use here a 10-member average of CESM2(CAM6) as well,
327 because ensemble size does affect skill (e.g., Sun et al., 2020). Therefore, in selected figures, we
328 also show CESM1(CAM5) and CESM2(CAM6) skill based on a 5-member ensemble, because

329 that is what the CESM2(WACCM6) skill assessment is based on. Richter et al. (2020) showed
330 that the 2-meter temperature and precipitation skill of CESM1(CAM5) was very similar to the
331 NOAA operational CFSv2 model and higher than those of most other models participating in
332 SubX. Surface temperature and precipitation prediction skill is similar between the CFSv2 model
333 and the European Centre for Medium-Range Weather Forecasts (ECMWF)Variable Resolution
334 Ensemble Prediction System monthly forecast system (Wang & Robertson 2019), hence broadly
335 speaking skill similar to CESM1(CAM5) implies prediction skill comparable to other operational
336 models.

337

338 **3.1 2-meter temperature and precipitation prediction skill**

339 Figures 2a-c show the anomaly correlation coefficients (ACC) for 2-meter (2m)
340 temperature for December, January, and February (DJF) for weeks 1-2, 3-4, and 5-6 for CESM2.
341 The NOAA Climate Prediction Center (CPC) Global Daily Temperature dataset at the $0.5^{\circ}\times 0.5^{\circ}$
342 resolution is used as a verification dataset. Both for observations and simulations, the average
343 daily temperature is calculated as the average of the daily maximum and minimum temperature.
344 Similarly to what was done for CESM1 in Richter et al. (2020), ACC values are shown in colors
345 only when they are significantly different from zero at the 95% confidence level or for $\text{ACC} >$
346 0.2. The significance level is calculated using a total sample size of 221, based on 13 start dates
347 per year over 17 years (1995 to 2015) considered here. Subsequently, we assume a 2-week
348 decorrelation time, and resulting in 110.5 independent samples. There are hence 108 degrees of
349 freedom (number of independent samples minus 2), leading to a correlation equal or greater than
350 0.2 being significant at the 95% level using a two-tailed Student's t-test (Wilks, 2011). Because
351 Richter et al. (2020) showed that nearly all the values over this threshold exceed the persistence
352 forecast, a persistence forecast is not repeated here. Figures 2a-c show declining ACC values

353 with forecast lead time reflecting a loss of deterministic skill with increasing forecast lead time.

354 The globally averaged DJF ACC for 2m temperature over all land areas is ~ 0.3 for weeks 3-4

355 and 0.2 for weeks 5-6 with higher values over the northern part of South America (ACC of ~ 0.5)

356 to 0.6 through weeks 5-6) and the lowest values over north and north-eastern Asia. The

357 differences of DJF 2m temperature ACC between CESM2(CAM6) and CESM1(CAM5) and

358 between CESM2(CAM6) and CESM2(WACCM) are given in Figs. 2d-f and Figs. 2g-i,

359 respectively. Only values that exceed the 95% confidence level using the Fisher z transform

360 (e.g., Zar, 2014) are shown. Figures 2d-2f show that DJF ACC for 2m temperature in

361 CESM2(CAM6) is overall very similar to that of CESM1(CAM5) for the majority of the world's

362 land regions, with the only exceptions being regions of decreased skill over parts of north-east

363 and southernmost Asia, and southernmost part of India for weeks 3-4 and 5-6. Figures 2g-2i

364 reveal that the DJF 2m temperature ACC for CESM2(WACCM6) is also very similar to that of

365 CESM2, demonstrating that the whole atmosphere version of CESM2 does not fundamentally

366 change the surface prediction skill of the model. There are a few land regions for which the DJF

367 2m temperature ACC is statistically significantly different for CESM2(WACCM6) as compared

368 to CESM2, most evident in weeks 5-6. These include parts of North America for which

369 CESM2(CAM6) is showing higher skill than CESM2(WACCM6), and eastern Asia where

370 higher skill is seen in CESM2(WACCM6) as compared to CESM2(CAM6). A detailed

371 investigation (beyond the scope of this paper) is needed to elucidate whether these differences

372 can be attributed to differences either in the representation of the stratosphere or in ocean and

373 atmosphere initialization procedures between the two configurations.

374 Figure 3 shows ACC of 2m temperature over land for June, July, August (JJA) average.

375 Comparison to CESM2(WACCM6) is not possible for this season due to the limited range of

376 reforecast start dates for that model version. The overall ACC of JJA 2m temperature is a little
377 smaller as compared to that for DJF. The ACC values are the largest in northern South America
378 and tropical Africa for weeks 3-4 and weeks 5-6 (Figs. 3b,c). The differences between ACC in
379 CESM2(CAM6) and CESM1(CAM5) are very small as shown in Figs 3d-3f. Figures S1 and S2
380 show the 2m temperature ACC for March, April, May (MAM) and September, October, and
381 November (SON) averages respectively. In MAM, CESM2(CAM6) shows a statistically
382 significant degradation of 2m temperature prediction skill over Eurasia and Alaska by ~0.2 for
383 weeks 3-4 and weeks 5-6 over CESM1(CAM5). In SON, there is very little difference between
384 the 2m temperature ACC for CESM2(CAM6) and CESM1(CAM5), as well as between
385 CESM2(WACCM6).

386 Figure 4 compares the DJF and JJA 2m temperature ACC averaged over all land areas and
387 over North America. DJF ACC of 2m temperature is ~ 0.6 for weeks 1-2, ~ 0.3 for weeks 3-4,
388 and < 0.2 for weeks 5-6 for global land for all the CESM versions considered here (Figure 4a).
389 DJF ACC of 2m temperature over North America is ~0.7 for weeks 1-2, ~0.3 for weeks 3-4, and
390 ~0.15 for weeks 5-6. JJA ACCs of 2m temperature for both global and North America land are
391 ~0.1 lower for weeks 1-2 and 3-4 as compared to DJF, while they are comparable to those of
392 DJF for weeks 5-6. There are overall small differences in 2m temperature ACCs between the
393 various model versions considered, as well as between ACCs calculated for an ensemble size of
394 5 vs 10 for CESM1(CAM5) and CESM2(CAM6) for both DJF and JJA. Although there are
395 small differences between CESM1(CAM5) and CESM2(CAM6) in DJF and JJA ACCs over
396 North America and global land, the application of the Fisher z transform to these values showed
397 that none of the differences between ACC values depicted by individual bars in Figure 4 are
398 statistically significant.

399 Figures 5a-c and 6a-c show the ACC for precipitation for DJF and JJA for
400 CESM2(CAM6). Precipitation prediction skill at subseasonal timescales (Figs. 5b,c) is quite low
401 as compared to the 2m temperature, with ACC values on average of ~ 0.1 for weeks 3-4 and <
402 0.05 for weeks 5-6 consistent with previous findings (Pegion et al., 2019, Richter et al., 2020).
403 Similarly to 2m temperature skill, precipitation skill is slightly higher in northern South America
404 and parts of Africa in weeks 3-4 in CESM2(CAM6) as compared to other land areas, reaching
405 ACC values of 0.3-0.4 over small regions (Figs. 5b,6b). There is little difference in DJF ACC of
406 precipitation between CESM2(CAM6) and CESM1(CAM5), and between CESM2(CAM6) and
407 CESM2(WACCM6). In JJA (Figure 6), the overall precipitation skill over land is even lower
408 than in DJF with the exception of Australia. In CESM2, for both weeks 3-4 and weeks 5-6 the
409 ACC of precipitation is ~ 0.3 - 0.5 over most of Australia, showing that CESM2(CAM6) is
410 skillful in that region. CESM1(CAM5) already had significant ACC over Australia in JJA
411 (Richter et al., 2020), so this skill has increased in CESM2(CAM6) especially for weeks 5-6
412 (Figure 6f). Figure 7 summarizes the precipitation prediction skill for DJF and JJA for all the
413 models considered in this study. Averaged over global land and North America the ACC of
414 precipitation is greater than zero but smaller than 0.1 for weeks 3-4 and weeks 4-5. ACC values
415 less than 0.1 imply that precipitation is generally not predictable on the subseasonal timescales,
416 except for very few selected regions discussed above.

417

418 **3.2 Spread and error characteristics for 2m temperature**

419 To shed some light on the ensemble characteristics of our S2S forecasts, we compute the
420 RMSE of the ensemble mean and the ensemble spread (Figure 8). Similarly to the ACC, the
421 RMSE over North American land is markedly higher in winter than in summer and decreases

423 slightly if the ensemble size is increased from 5 to 10 members. Unlike Figure 4, we do not
424 detect the same rapid decrease in skill between week 1-2 and 3-4 forecasts. This points to the fact
425 that week 1-2 reforecasts have a high pattern correlation with the verifying analysis but might
426 have problems capturing the anomaly magnitudes.

427 The ensemble spread is computed as lead-time dependent standard deviation of all
428 members around the ensemble mean and is shown as hatched bars in Figure 8. For a reliable
429 ensemble system, the ensemble spread should inform the state-dependent predictability of the
430 system and the spread and error of the ensemble mean should have the same magnitude (e.g.
431 Leutbecher and Palmer, 2008). However, most ensemble systems are overconfident (e.g., Berner
432 et al. 2015, Leutbecher et al. 2017) and the spread predicting the uncertainty of the forecast is
433 smaller than the RMSE.

434 Such underdispersion is also evident in our reforecasts. In weeks 1-2, regardless of the
435 season, or land area average, the spread is under-dispersive by at least 40% (Fig 8.). The
436 underdispersion improves for longer lead times but forecasts remain markedly overconfident for
437 all experiments. The differences between the different CESM configurations are small for JJA,
438 but for DJF, CESM1(CAM5) creates consistently more spread than CESM2(CAM6) or
439 CESM2(WACCM) over North American land. Increasing the ensemble size has a more
440 pronounced effect on the spread than the RMSE error. This indicates that the value of the
441 ensemble might lie in the improved representation of uncertainty rather than improved
442 deterministic skill.

443
444
445 **3.3 MJO and NAO prediction skill**
446

447 The MJO and the NAO are key drivers of extreme weather on subseasonal timescales and
448 believed to be key sources of subseasonal predictability. To evaluate the MJO prediction skill,
449 the Real-time Multivariate MJO (RMM; Wheeler & Hendon, 2004) index is calculated with the
450 200 hPa and 850 hPa daily zonal wind from ECMWF Reanalysis v5 (ERA5; Hersbach et al.,
451 2020) and the Outgoing Longwave Radiation (OLR) from NOAA Advanced Very High-
452 Resolution Radiometer (Liebmann & Smith 1996). Predicted RMM indices are calculated by
453 projecting the forecast anomalies for those fields onto the associated observed EOF eigenvectors
454 (Kim et al., 2018). Then, the RMM index bivariate ACCs are computed between the predicted
455 and observed RMM1 and RMM2 indices as a function of forecast lead days. The MJO prediction
456 skill is assessed during boreal winter with the reforecasts initialized during November-March
457 (NDJFM). Due to the limited sample size, all days are selected as MJO events without any
458 discrimination of the initial MJO amplitude. Figure 9 shows ACC as a function of forecast lead
459 days where ACC of 0.5 is explicitly denoted as it is often used as a skill threshold (e.g., Rashid et
460 al., 2011). The figure clearly demonstrates that the MJO in CESM2(CAM6) and
461 CESM2(WACCM6) is predictable out to 25 days, which is longer than the predictability of the
462 MJO for most of the SubX models (not shown), but less than than the MJO predictability of out
463 to 33 days in the ECMWF-CY43R system (Kim et al., 2019b). The ACC of the MJO in
464 CESM1(CAM5) is slightly higher compared to CESM2(CAM6) and CESM2(WACCM6),
465 however, none of the skill differences are statistically significant based on the Fisher z transform.
466 There is also very little difference in the overall MJO skill between CESM2(CAM6) and
467 CESM2(WACCM6) (when the same ensemble size is considered) indicating that neither the
468 extension of the model top into the middle atmosphere nor the different ocean initialization in
469 CESM2(WACCM6) as compared to CESM2(CAM6) affect MJO prediction skill.

470 The NAO is a key driver of winter extreme weather over Europe and North America
471 (Hurrell, 1995; Scaife et al., 2008). It is predictable on weather (< 2 weeks) timescales and
472 seasonal timescales (e.g., Riddle et al., 2013, Scaife et al. 2014a), however its predictability on
473 subseasonal timescales is less certain and has not been explored extensively. Zuo et al. (2016)
474 found the NAO to be predictable only out to ~ 9 days using the Beijing Climate Center
475 Atmospheric General Circulation Model version 2.2 (BCC AGCM2.2). Pegion et al. (2019)
476 showed that NAO skill was high ($ACC > 0.5$) through week 2 in all the SubX models. Richter et
477 al. (2020) found that the ACC of NAO in CESM1(CAM5) was 0.5 at week 3 and 0.4 at week 4
478 (10-member ensemble). Sun et al. (2020) found that an increase in ensemble size to 20 enhances
479 the NAO prediction skill, with an NAO ACC of 0.51 for weeks 3 to 6 in boreal winter in
480 CESM1(CAM5). The prediction skill of the NAO in the various CESM configurations is shown
481 in Figure 10. The NAO index was obtained by first calculating EOF analysis of ERA-Interim
482 monthly (NDJFM) sea level pressure (SLP) anomalies over the Atlantic sector (20°N – 80°N ,
483 90°W – 40°E) and treating the leading EOF pattern as the NAO. The NAO index was then
484 calculated by projecting the SLP anomaly in the reanalysis and reforecasts that were initialized
485 during NDJFM onto the leading EOF. The week 3-4 NAO ACC is above or close to 0.5 for all
486 the CESM versions considered here, similar to the skill in ECMWF and NCEP reforecasts
487 (Wang & Robertson, 2018). ACC of CESM1(CAM5) based on a 10-member ensemble and
488 CESM2(WACCM6) based on a 5-member ensemble have the highest skill at week 3-4, however,
489 with the current reforecast sample size, these skill values are not significantly different than the
490 ACC for CESM2(CAM6) or CESM1(CAM5) based on a 5-member ensemble. The NAO skill
491 for CESM2(WACCM6) is very close to the NAO skill for CESM1(CAM5) at weeks 5-6, and
492 substantially higher than that for CESM2(CAM6) with a 5-member ensemble. This could

493 possibly be attributed to a better resolved stratosphere in CESM2(WACCM6), but as with other
494 comparisons shown throughout this manuscript, due to the limited sample size, these differences
495 are not statistically significant.

496

497 **3.4 Stratosphere-troposphere coupling**

498 The stratosphere, and in particular, stratosphere-troposphere coupling during SSWs may
499 be an important source of subseasonal predictability. SSWs are associated with enhanced surface
500 pressure over the polar cap, and they tend to be followed by warm temperatures over
501 Northeastern Canada and Greenland, cold temperatures over Eurasia, and enhanced precipitation
502 over Western Europe (Butler et al., 2017, Domeisen & Butler 2020, Baldwin et al., 2020). This
503 coupling between tropospheric weather and sudden warmings is often summarized by the time
504 evolution of the annular modes (Baldwin and Dunkerton 2001), or nearly equivalently, the
505 standardized polar cap geopotential anomalies (Figure 11). During the onset of an SSW,
506 anomalously positive geopotential anomalies descend from the middle to the lower stratosphere,
507 where they can linger for over one month. Their descent to the surface manifests itself as
508 changes to the Arctic Oscillation (AO) or the NAO over the Atlantic sector.

510 Here, the standardized polar cap geopotential anomalies in MERRA-2 (Figure 11a) and
511 in CESM2(WACCM6) and CESM2(CAM6) reforecasts that predicted a major SSW within 7
512 days of the SSW central date in MERRA-2 reanalysis (Figs. 11b,c) are composited with respect
513 to the central date of the observed or reforecasted SSW. We emphasize that only reforecasts that
514 predicted an SSW were selected to assess the models' ability to capture surface impacts. The
515 central date of an SSW is the first day when the zonal-mean zonal wind at 60°N and 10 hPa
516 becomes negative, with 14 SSW events in the reforecast period. The central dates of the

517 observed events are: (1) Feb 26, 1999; (2) Feb 11, 2001; (3) Dec 30, 2001; (4) Feb 17, 2002; (5)
518 Jan 18, 2003; (6) Jan 5, 2004; (7) Jan 21, 2006; (8) Feb 24, 2007; (9) Feb 22, 2008; (10) Jan 24,
519 2009; (11) Feb 9, 2010; (12) Jan 6, 2013; (13) Feb 12, 2018; and (14) Jan 2, 2019. Figure 12
520 shows that while the magnitude of the positive geopotential anomalies during the SSW events is
521 comparable between MERRA-2 and the CESM2(WACCM6) and CESM2(CAM6) reforecasts,
522 the positive anomalies in the lower stratosphere do not linger as long in the reforecasts, only out
523 to day 35 and 39, respectively. However, the positive surface geopotential anomalies linger for 4
524 weeks after the central date of a SSW in the reforecasts and in MERRA-2, indicating that the
525 coupling of the events with the troposphere is comparable (Baldwin et al., 2021). The squared
526 pattern correlations of the composited geopotential anomalies between the CESM2(WACCM6)
527 and CESM2(CAM6) reforecasts and MERRA-2 are similarly high at 0.80 and 0.77 respectively.
528 In contrast, the averages of the individual reforecast pattern correlations with their respective
529 SSW event in MERRA-2 are substantially lower with 0.39 for CESM2(WACCM) and 0.25 for
530 CESM2(CAM6). In summary, CESM2(WACCM6) reforecasts of the polar cap geopotential
531 anomalies following an SSW are somewhat more consistent with those of MERRA-2 than in
532 CESM2(CAM6) reforecasts.

533

3.5 Mesosphere and lower thermosphere prediction

534 Initial investigations by Wang et al. (2014) and Pedatella et al. (2018b) demonstrated the
535 potential to predict the MLT variability during the 2009 SSW event, though these studies were
536 limited to a single event. The CESM2(WACCM6) reforecasts provide the opportunity to perform
537 more detailed investigations into the MLT predictability during SSWs. Davis et al. (2021)
538 showed that SSW predictability at lead times of one to two weeks is enhanced in reforecasts
539

541 initialized with weaker stratospheric jets. Figure 12 presents an analysis of SSW predictability
542 using a composite of the zonal-mean temperature between 70°-90°N from 14 major SSW events
543 that are captured in the time periods of CESM2(WACCM6) reforecasts and SSWs from
544 WACCM Specified Dynamics simulations with thermosphere-ionosphere eXtension
545 (WACCMX-SD; Liu et al., 2018) are used for verification (Figure 12a). Figures 12b-e show the
546 composites for reforecasts initialized 15, 10, 5, and 0 days prior to the SSW central date. Note
547 that the results in Figure 12 are based on compositing the reforecasts regardless of whether they
548 successfully forecast a SSW, and we consider reforecasts initialized within +/- 3 days of the
549 specified lag for the composites (i.e., a lag of -10 includes reforecasts initialized 7-13 days prior
550 to the SSW).

551 Several distinct features of the middle atmosphere (stratosphere \sim 100 to 0.5 hPa or \sim 10
552 to 50 km; mesosphere: 0.5 hPa to 10^{-3} hPa \sim 50 to 90 km, lower thermosphere: above 10^{-3} hPa)
553 response to SSWs can be seen in Figure 12a. This includes a mesosphere cooling that begins
554 right after the central date of the SSW between $\sim 10^{-1}$ and 10^{-3} hPa that accompanies the warming
555 in the stratosphere, as well as the reformation of the stratopause at high altitudes following the
556 SSW. We note that formation of an elevated stratopause following an SSW does not always
557 occur (Chandran et al., 2013), though it is present in the vast majority of the events considered
558 here, thus appearing in the composite analysis. The CESM2(WACCM6) reforecasts indicate that
559 the formation of an elevated stratopause and the mesosphere cooling can be predicted \sim 10-15
560 days in advance of the SSW, though the altitude of the elevated stratopause is too low in these
561 early predictions. The reforecasts initialized closer to the SSW (Figure 12d) and near the SSW
562 onset (Figure 12e) capture the mesosphere cooling and elevated stratopause with higher fidelity
563 when comparing to WACCMX-SD. These results provide an initial demonstration that the MLT

564 variability can be predicted ~5-15 days in advance of SSWs. The MLT variations during SSW
565 generate subsequent variations in the ionosphere and thermosphere, and the results in Figure 12
566 thus suggest that it may be possible to also forecast the upper atmosphere variability ~10 days in
567 advance of an SSW.

568

569

570 **3.6 Limitations of current framework for chemistry prediction**

571 As CESM2(WACCM6) includes a comprehensive tropospheric and middle atmospheric
572 chemistry module, we were hopeful that the current model framework could also be used to
573 explore the predictability of stratospheric chemistry such as water vapor and ozone. However,
574 we have discovered that nudging CESM2(WACCM6) to MERRA-2 with a 1-hourly timescale
575 introduces significant deviations between modeled and observed water vapor. This is illustrated
576 in Figure 13 which shows the time evolution of the stratospheric tropical water vapor, also
577 known as the “tape recorder” (Mote et al. 1996), for WACCM6-SD simulation (used to initialize
578 CESM2(WACCM6) reforecasts) and Microwave Limb Sounder (MLS) observations (Lambert et
579 al., 2015). Figure 13a reveals that stratospheric water vapor concentrations in WACCM6-SD are
580 approximately double the observed concentration. Additionally, the water vapor tape recorder
581 indicates faster ascent in WACCM6-SD, such that the simulated water vapor leads the
582 observations as seen in the 100 hPa and 70 hPa time series (Figure 13b).

584 We have performed several sensitivity experiments with WACCM6-SD, including an
585 experiment in which we lowered the nudging top from 60 km to 50 km and another experiment
586 in which we increased the nudging timescale from 1 to 2 hours. We found that the first
587 experiment had no effect on the simulation of water vapor, whereas the second experiment

588 decreased the value of tropical lower stratospheric water vapor by about 15%, making the time
589 evolution of water vapor closer to observations. It is possible that the 2-hour nudging results in a
590 colder and higher tropopause or weaker recirculation of water vapor-rich air from the
591 midlatitudes, both of which would reduce water vapor within the tape recorder. It is also possible
592 that temperature nudging acts as diabatic heating and artificially changes the strength of the
593 meridional circulation (Miyazaki et al., 2005). This could decrease the transit time of water
594 vapor-rich tropospheric air through the tropical tropopause layer, thereby decreasing the amount
595 of dehydration that can occur. An even longer nudging timescale in the stratosphere may
596 improve the representation of stratospheric chemistry in the S2S reforecasts/forecasts with
597 CESM2(WACCM6) and we will explore this in the future further.

598

599 **4 Summary and Conclusions**

600 We have described here a fully coupled Earth system subseasonal prediction framework
601 with CESM2(CAM6) and CESM2(WACCM6) developed for research purposes.
602 CESM2(CAM6) and CESM2(WACCM6) are the newest versions of the NCAR Earth system
603 model used in CMIP6, and the two configurations differ in the atmospheric model components.
604 CESM2(CAM6) has a top near 40 km, whereas CESM2(WACCM6) extends up to ~ 140 km and
605 includes fully interactive tropospheric and stratospheric chemistry. Both configurations include
606 prognostic aerosols. Subseasonal reforecasts were carried out following the SubX protocol for
607 years 1999 - 2020 with weekly start dates for each year for CESM2, and with weekly start dates
608 only between September and March for CESM2(WACCM6). Near real-time forecasts with the
609 model have been running since September 2020 for CESM2(WACCM6) and since April 2021
610 for CESM2.

611 We demonstrated that the prediction skill of 2m temperature and precipitation as well as
612 of the MJO and NAO are comparable to the prediction skill for these variables in CESM1 and
613 similar to the skill seen in some operational models (NOAA's CFSv2 and ECMWF). The high
614 subseasonal prediction skill of this research framework, along with extensive output obtained for
615 all model components, makes it an excellent tool for studies of subseasonal predictability. We
616 demonstrated that stratospheric-tropospheric coupling during SSW events is well represented in
617 CESM2(CAM6) and CESM2(WACCM6), which implies that both configurations will likely
618 capture well surface impacts of these events. This will be investigated in future studies.
619 CESM2(WACCM6) can also be used for predictability research of the dynamics of the
620 stratosphere and the mesosphere and lower-thermosphere region. We further demonstrated that
621 variability in the MLT region is predictable ~ 10 days in advance of SSWs.

622 In general, the subseasonal prediction skill of tropospheric atmospheric variables is very
623 similar between CESM2(CAM6) and CESM2(WACCM6). Therefore, the differences either in
624 ocean and atmosphere initialization procedures or differences in model lids and representation of
625 the stratosphere have not translated into many significant differences in prediction skills of the
626 variables examined here. Nevertheless, the noted differences in skill include higher DJF 2m
627 temperature skill in eastern Asia in CESM2(WACCM6) as compared to CESM2(CAM6), and
628 higher 2m temperature skill in parts of North America in CESM2(CAM6), both for weeks 5-6.
629 Stratospheric-tropospheric coupling is well-represented in both models, however, the polar cap
630 geopotential anomalies following an SSW are more consistent with observations in
631 CESM2(WACCM6) as compared to CESM2. The impact of this difference on predictability of
632 surface extreme weather associated with SSWs will be investigated in future work.

633 CESM2(CAM6) and CESM2(WACCM6) are freely available for use by the community.

634 The reforecast sets described here are publicly available and are designed to serve as a basis for
635 future experiments elucidating sources of subseasonal predictability. The near real-time
636 forecasts are contributing to the NOAA week 3-4 outlook. The extensive output from the
637 atmospheric, land, ocean and sea-ice components of the model may open new avenues of
638 research.

639

640

Acknowledgements and Data

641

642 This work was supported by the National Oceanic and Atmospheric Administration's Weather
643 Program Office/Climate Test Bed Program, and by the National Center for Atmospheric
644 Research (NCAR), which is a major facility sponsored by the National Science Foundation
645 (NSF) under Cooperative Agreement 1852977. Portions of this study were supported by the
646 Regional and Global Model Analysis (RGMA) component of the Earth and Environmental
647 System Modeling Program of the U.S. Department of Energy's Office of Biological &
648 Environmental Research (BER) via NSF Interagency Agreement 1844590. Portions of this study
649 were supported by the NOAA Office of Weather and Air Quality Research Programs (OWAQ)
650 (Subseasonal to Seasonal) under grant NA19OAR4590156. Computing and data storage
651 resources, including the Cheyenne supercomputer (doi:10.5065/D6RX99HX), were provided by
652 the Computational and Information Systems Laboratory (CISL) at NCAR. We thank the
653 National Aeronautics and Space Administration (NASA) for making the FP-IT data available to
654 us for this project. MERRA-2 is available from NASA's Global Modeling and Assimilation
655 office at <https://gmao.gsfc.nasa.gov/reanalysis/MERRA-2/>. CPC Global Temperature data
656 provided by the NOAA/OAR/ESRL PSL, Boulder, Colorado, USA, from their Web site at
657 <https://psl.noaa.gov/data/gridded/data.cpc.globaltemp.html>. CESM2(CAM6) and
658 <https://psl.noaa.gov/data/gridded/data.cpc.globaltemp.html>.

659 CESM2(WACCM6) reforecast outputs are available for download from the NCAR Climate Data
660 Gateway and can be accessed via the following DOI's: <https://doi.org/10.5065/0s63-m767> and
661 <https://doi.org/10.5065/ekns-e430> respectively.

662
663 **References**
664

- 665 Beljaars, A. C. M., Brown, A. R., & Wood, N. (2004). A new parameterization of turbulent
666 orographic form drag. *Quarterly Journal of the Royal Meteorological Society*, 130, 1327–
667 1347. <https://doi.org/10.1256/qj.03.73>
- 668 Baldwin, Mark P., & T. J. Dunkerton (2001). Stratospheric harbingers of anomalous weather
669 regimes. *Science*, 294.5542, 581-584, 10.1126/science.1063315.
- 670 Baldwin, M. P., Ayarzagüena, B., Birner, T., Butchart, N., Butler, A. H., Charlton-Perez, A. J., et
671 al. (2021). Sudden stratospheric warmings. *Reviews of Geophysics*, 59, e2020RG000708.
672 <https://doi.org/10.1029/2020RG000708>
- 673 Berner, J., Fossell K. R., Ha S.-Y., Hacker J. P. & Snyder C. (2015). Increasing the skill of
674 probabilistic forecasts: Understanding performance improvements from model-error
675 representations. *Monthly Weather Review*, 143.4, 1295-1320. <https://doi.org/10.1175/MWR-D-14-00091.1>
- 677 Boer, G. J., & Hamilton, K. QBO influence on extratropical predictive skill, *Clim. Dyn.*, 31,
678 987–1000 (2008).
- 679 Butler, A. H., Sjoberg, J. P., Seidel, D. J., & Rosenlof, K. H. (2017). A sudden stratospheric
680 warming compendium. *Earth System Science Data*, 9, 63–76, <https://doi.org/10.5194/essd-9-63-2017>.

- 682 Chandran, A., Collins, R. L., Garcia, R. R., Marsh, D. R., Harvey, V. L., Yue, J., & de la Torre, L. (2013). A
683 climatology of elevated stratopause events in the whole atmosphere community climate model, *J.
684 Geophys. Res. Atmos.*, 118, 1234- 1246, doi:[10.1002/jgrd.50123](https://doi.org/10.1002/jgrd.50123).
- 685 Danabasoglu, G., Bates, S. C., Briegleb, B. P., Jayne, S. R., Jochum, M., Large, W. G., et al.
686 (2012). The CCSM4 ocean component. *Journal of Climate*, 25, 1361–1389.
687 <https://doi.org/10.1175/JCLI-D-11-00091.1>
- 688 Danabasoglu, G., Lamarque, J.-F., Bacmeister, J., Bailey, D. A., DuVivier, A. K., Edwards, J., et
689 al. (2020). The Community Earth System Model Version 2 (CESM2). *Journal of Advances in
690 Modeling Earth Systems*, 12, e2019MS001916. <https://doi.org/10.1029/2019MS001916>
- 691 Davis, A. N., J. H. Richter, J. Edwards, & A. A. Glanville (2021): A positive zonal wind
692 feedback on sudden stratospheric warming development revealed by CESM2 (WACCM6)
693 reforecasts, *Geophysical Research Letters*, 48,
694 e2020GL090863. <https://doi.org/10.1029/2020GL090863>
- 695 de Andrade, F. M., Coelho, C. A. S., & Cavalcanti, I. F. A. (2019). Global precipitation hindcast
696 quality assessment of the subseasonal to seasonal (S2S) prediction project models. *Climate
697 Dynamics*, 52(9-10), 5451–5475. <https://doi.org/10.1007/s00382-018-4457-z>
- 698 Diro, G. T., & Lin, H. (2020). Subseasonal Forecast Skill of Snow Water Equivalent and Its Link
699 with Temperature in Selected SubX Models, *Weather and Forecasting*, 35(1), 273-284.
- 700 Domeisen, D.I.V. & Butler, A.H. (2020). Stratospheric drivers of extreme events at the Earth's
701 surface. *Communications Earth and Environment*, 1, 59, [https://doi.org/10.1038/s43247-020-00060-z](https://doi.org/10.1038/s43247-020-
702 00060-z)
- 703 Ford, T.W., Dirmeyer, P.A. & Benson, D.O. Evaluation of heat wave forecasts seamlessly across
704 subseasonal timescales. *npj Climate and Atmospheric Science* 1, 20 (2018).
705 <https://doi.org/10.1038/s41612-018-0027-7>

- 706 Gelaro, R., McCarty, W., Suárez, M. J., Todling, R., Molod, A., Takacs L., et al. (2017). The
707 Modern-Era Retrospective Analysis for Research and Applications, Version 2 (MERRA-2).
708 *Journal of Climate*, **30**, 5419–5454, <https://doi.org/10.1175/JCLI-D-16-0758.1>.
- 709 Gettelman, A., & Morrison, H. (2015). Advanced two-moment bulk microphysics for global
710 models. Part I: Off-line tests and comparison with other schemes. *Journal of Climate*, **28**,
711 1268–1287. <https://doi.org/10.1175/JCLI-D-14-00102.1>
- 712 Gettelman, A., Mills, M. J., Kinnison, D. E., Garcia, R. R., Smith, A. K., Marsh, D. R., et al.
713 (2019). The Whole Atmosphere Community Climate Model version 6 (WACCM6). *Journal*
714 *of Geophysical Research: Atmospheres*, **124**(23), 12,380–12,403. <https://doi.org/10.1029/2019JD030943>
- 716 Golaz, J.-C., Larson, V. E., & Cotton, W. R. (2002). A PDF-based model for boundary layer
717 clouds. Part I: Method and model description. *Journal of the Atmospheric Sciences*, **59**,
718 3540–3551.
- 719 Griffies, S. M., Danabasoglu G., Durack P. J., Adcroft A. J., Balaji V., Böning C. W., et al.
720 (2016). OMIP contribution to CMIP6: Experimental and diagnostic protocol for the physical
721 component of the ocean model intercomparison project. *Geoscience Model Development*, **9**,
722 3231–3296, <https://doi.org/10.5194/gmd-9-3231-2016>.
- 723 Zhu H., H. Chen, Y. Zhou & X. Dong (2019). Evaluation of the subseasonal forecast skill of
724 surface soil moisture in the S2S database, *Atmospheric and Oceanic Science Letters*, **12**:6,
725 467-474, DOI: [10.1080/16742834.2019.1663123](https://doi.org/10.1080/16742834.2019.1663123)
- 726 Hersbach, H., Bell, B., Berrisford, P., Hirahara S., Horányi A., Muñoz-Sabater J., et al. (2020).
727 The ERA5 global reanalysis. *Quarterly Journal of Royal Meteorological Society*, **146**, 1999–
728 2049, <https://doi.org/10.1002/qj.3803>

- 729 Hunke, E. C., Hebert, D. A., & Lecomte, O. (2013). Level-ice melt ponds in the Los Alamos sea
730 ice model, CICE. *Ocean Modelling*, 71, 26–42.
- 731 <https://doi.org/10.1016/j.ocemod.2012.11.008>
- 732 Hunke, E. C., Lipscomb, W. H., Turner, A. K., Jeffery, N., & Elliott, S. (2015). CICE: The Los
733 Alamos Sea Ice Model. Documentation and Software User's Manual. Version 5.1. T-3 Fluid
734 Dynamics Group, Los Alamos National Laboratory, Tech. Rep. LA-CC-06-012.
- 735 Hurrell, J. W., (1995). Decadal trends in the North Atlantic Oscillation: Regional temperatures
736 and precipitation. *Science*, 269, 676–679, <https://doi.org/10.1126/science.269.5224.676>.
- 737 Jackson, D. R., Fuller-Rowell, T. J., Griffin, D. J., Griffith, M. J., Kelly, C. W., Marsh, D. R., & Walach, M.-
738 T. (2019). Future directions for whole atmosphere modeling: Developments in the context of space
739 weather. *Space Weather*, 17, 1342– 1350. <https://doi.org/10.1029/2019SW002267>
- 740 Kim, H., Vitart, F., & Waliser, D. E. (2018). Prediction of the Madden–Julian Oscillation: A
741 Review. *Journal of Climate*, 31(23), 9425–9443. <https://doi.org/10.1175/JCLI-D-18-0210.1>
- 742 Kim, H., Richter, J. H., & Martin, Z. (2019a). Insignificant QBO-MJO prediction skill
743 relationship in the SubX and S2S subseasonal reforecasts. *Journal of Geophysical Research:*
744 *Atmospheres*, 124, 12,655–12,666. <https://doi.org/10.1029/2019JD031416>
- 745 Kim, H., Janiga, M. A., & Pégion, K. (2019b). MJO propagation processes and mean biases in
746 the SubX and S2S reforecasts. *Journal of Geophysical Research: Atmospheres*, 124, 9314–
747 9331. <https://doi.org/10.1029/2019JD031139>
- 748 Lambert, A., Read, W. & Livesey, N. (2015). MLS/Aura Level 2 Water Vapor (H₂O) Mixing
749 Ratio V004, Greenbelt, MD, USA, *Goddard Earth Sciences Data and Information Services*
750 *Center (GES DISC)*, 10.5067/Aura/MLS/DATA2009
- 751 Larson, V. E., (2017). CLUBB-SILHS: A parameterization of subgrid variability in the
752 atmosphere. arXiv:1711.03675v2 [physics.ao-ph].

- 753 Lawrence, D. M., Fisher, R. A., Koven, C. D., Oleson, K. W., Swenson, S. C., Bonan, G., et al.
754 (2019). The Community Land Model Version 5: Description of new features, benchmarking,
755 and impact of forcing uncertainty. *Journal of Advances in Modeling Earth Systems*, 11,
756 4245–4287. <https://doi.org/10.1029/2018MS001583>
- 757 Leutbecher, M., & Tim N. Palmer (2008). Ensemble forecasting. *Journal of computational
758 physics*, 3515-3539.
- 759 Leutbecher, M., Lock S.-J., Ollinaho P., Lang, S. T.K., Balsamo, G., Bechtold P., et al. (2017).
760 Stochastic representations of model uncertainties at ECMWF: State of the art and future
761 vision. *Quarterly Journal of the Royal Meteorological Society* 143.707 (2017): 2315-2339.
762 <https://doi.org/10.1002/qj.3094>
- 763 Levis, S., Badger, A., Drewniak, B., Nevison, C., & Ren, X. L. (2018). CLMcrop yields and
764 water requirements: Avoided impacts by choosing RCP 4.5 over 8.5. *Climatic Change*, 146,
765 501–515. <https://doi.org/10.1007/s10584-016-1654-9>
- 766 Li, F., Levis, S., & Ward, D. S. (2013). Quantifying the role of fire in the Earth system—Part 1:
767 Improved global fire modeling in the Community Earth System Model (CESM1).
768 *Biogeosciences*, 10, 2293–2314. <https://doi.org/10.5194/bg-10-2293-2013>
- 769 Li, F., & Lawrence, D. M. (2017). Role of fire in the global land water budget during the
770 twentieth century due to changing ecosystems. *Journal of Climate*, 30, 1893–1908.
771 <https://doi.org/10.1175/JCLI-D-16-0460.1>
- 772 Lim, Y., Son, S., & Kim, D. (2018). MJO Prediction Skill of the Subseasonal-to-Seasonal
773 Prediction Models, *Journal of Climate*, 31(10), 4075-4094. Retrieved Feb 14, 2021, from
774 <https://journals.ametsoc.org/view/journals/clim/31/10/jcli-d-17-0545.1.xml>

- 775 Lim, Y., Son, S.-W., Marshall, A. G., Hendon, H. H., & Seo, K.-H. (2019). Influence of the
776 QBO on MJO prediction skill in the subseasonal- to-seasonal prediction models. *Climate
777 Dynamics*, 1–15.
- 778 Lipscomb, W. H., Price, S. F., Hoffman, M. J., Leguy, G. R., Bennett, A. R., Bradley, S. L., et al.
779 (2019). Description and evaluation of the Community Ice Sheet Model (CISM) v. 2.1.
780 *Geoscientific Model Development*, 12, 387–424. <https://doi.org/10.5194/gmd-12-387-2019>
- 781 Liu, X., Ma, P. L., Wang, H., Tilmes, S., Singh, B., Easter, R. C., et al. (2016). Description and
782 evaluation of a new four-mode version of the Modal Aerosol Module (MAM4) within
783 Version 5.3 of the Community Atmosphere Model. *Geoscientific Model Development*, 9,
784 505–522. <https://doi.org/10.5194/gmd-9-505-2016>
- 785 Liu, H.-L., Bardeen, C. G., Foster, B. T., Lauritzen, P., Liu, J., Lu, G., Wang, W. et al., (2018). Development
786 and validation of the Whole Atmosphere Community Climate Model with thermosphere and ionosphere
787 extension (WACCM-X 2.0). *Journal of Advances in Modeling Earth Systems*, 10, 381– 402.
788 <https://doi.org/10.1002/2017MS001232>
- 789 Marshall, A. G., & Scaife, A. A. (2010): Improved predictability of stratospheric sudden
790 warming events in an atmospheric general circulation model with enhanced stratospheric
791 resolution, *Journal of Geophysical Research*, 115, D16114, doi:[10.1029/2009JD012643](https://doi.org/10.1029/2009JD012643)
- 792 Miyazaki, K., Iwasaki, T., Shibata, K., Deushi, M., & Sekiyama, T. T. (2005). The impact of
793 changing meteorological variables to be assimilated into GCM on ozone simulation with
794 MRI CTM, *Journal of the Meteorological Society of Japan. Ser. II*, 83, 909-918,
795 <https://doi.org/10.2151/jmsj.83.909>.
- 796 Moore, J. K., Doney, S. C., Kleypas, J. A., Glover, D. M., & Fung, I. Y. (2002). An intermediate
797 complexity marine ecosystem model for the global domain. *Deep Sea Research*, 49, 403–
798 462. [https://doi.org/10.1016/S0967-0645\(01\)00108-4](https://doi.org/10.1016/S0967-0645(01)00108-4)

- 799 Moore, J. K., Doney, S. C., & Lindsay, K. (2004). Upper ocean ecosystem dynamics and iron
800 cycling in a global three-dimensional model. *Global Biogeochemical Cycles*, 18, GB4028.
801 <https://doi.org/10.1029/2004GB002220>
- 802 Moore, J. K., Lindsay, K., Doney, S. C., Long, M. C., & Misumi, K. (2013). Marine Ecosystem
803 Dynamics and Biogeochemical Cycling in the Community Earth System Model
804 [CESM1(BGC)]: Comparison of the 1990s with the 2090s under the RCP4.5 and RCP8.5
805 scenarios. *Journal of Climate*, 26, 9291–9312. <https://doi.org/10.1175/JCLI-D-12-00566.1>
- 806 Mote, P. W., Rosenlof, K. H., McIntyre, M. E., Carr, E. S., Gille, J. C., Holton, J. R., et al. (1996). An
807 atmospheric tape recorder: The imprint of tropical tropopause temperatures on stratospheric water vapor,
808 *Journal of Geophysical Research*, 101(D2), 3989–4006, doi:[10.1029/95JD03422](https://doi.org/10.1029/95JD03422).
- 809 NAS, 2016: Next Generation Earth System Prediction: Strategies for Subseasonal to Seasonal
810 Forecasts. The National Academies Press, 350 pp., <https://doi.org/10.17226/21873>.
- 811 Oleson, K. W., & Feddema, J. (2019). Parameterization and surface data improvements and new
812 capabilities for the Community Land Model Urban (CLMU). *Journal of Advances in
813 Modeling Earth Systems*. <https://doi.org/10.1029/2018MS001586>
- 814 Pedatella, N. M., Liu, H.-L., Marsh, D. R., Raeder, K., Anderson, J. L., Chau, J. L., et al.
815 (2018a). Analysis and hindcast experiments of the 2009 sudden stratospheric warming in
816 WACCMX+DART. *Journal of Geophysical Research: Space Physics*, 123, 3131–3153.
817 <https://doi.org/10.1002/2017JA025107>
- 818 Pedatella, N. M., J. L. Chau, H. Schmidt, L. P. Goncharenko, C. Stolle, K. Hocke, V. L. Harvey,
819 B. Funke, and T. A. Siddiqui (2018). *EOS*. <https://eos.org/features/how-sudden-stratospheric-warming-affects-the-whole-atmosphere>
- 821 Pegion, K., Kirtman, B. P., Becker, E., Collins, D. C., LaJoie E., Burgman, R., Bell, R. et al.
822 (2019). The Subseasonal Experiment (SubX): A multimodel subseasonal prediction

- 823 experiment. *Bulletin of the American Meteorological Society*, 100, 2043–2060,
824 <https://doi.org/10.1175/BAMS-D-18-0270.1>.
- 825 Rashid, H. A., Hendon, H. H., Wheeler, M. C., & Alves, O. (2011). *Climate Dynamics*, 36(3-4),
826 649–661. <https://doi.org/10.1007/s00382-010-0754-x>
- 827 Richter, J. H., Sassi, F., & Garcia, R. R. (2010). Toward a Physically Based Gravity Wave
828 Source Parameterization in a General Circulation Model. *Journal of the Atmospheric
829 Sciences*, 67(1), 136–156. <https://doi.org/10.1175/2009JAS3112.1>
- 830 Richter, J. H., Pigion K., Sun L, Kim H., Caron J. M., Glanville A., et al. (2020). Subseasonal
831 prediction with and without a well-represented stratosphere in CESM1. *Weather and
832 Forecasting*, doi: <https://doi.org/10.1175/WAF-D-20-0029.1>.
- 833 Riddle, E. E., Butler, A. H., Furtado, J. C., Cohen, J. L., & Kumar, A. (2013). CFSv2 ensemble
834 prediction of the wintertime Arctic Oscillation, *Climate Dynamics*, 41, 1099–1116.
- 835 Saha, S., Moorthi S., Wu X., Wang J., Nadiga S., Tripp P., et al. (2014). The NCEP Climate
836 Forecast System Version 2. *Journal of Climate*, 27, 2185–2208,
837 <https://doi.org/10.1175/JCLI-D-12-00823.1>.
- 838 Scaife, A. A., C. K. Folland, L. V. Alexander, A. Moberg, & J. D. Knight (2008). European
839 climate extremes and the North Atlantic Oscillation. *Journal of Climate*, 21, 72–83,
840 <https://doi.org/10.1175/2007JCLI1631.1>.
- 841 Scaife, A., Arribas, A., Blockley, E., Brookshaw, A., Clark, R., Dunstone, N., et al. (2014).
842 Skillful long-range prediction of European and North American winters, *Geophysical
843 Research Letters*, 41, 2514–2519.
- 844 Scaife, A.A., Athanassiadou M., Andrews M., Arribas A., Baldwin M., Dunstone N., et al.
845 (2014b). Predictability of the quasi-biennial oscillation and its northern winter teleconnection

- 846 on seasonal to decadal timescales, *Geophysical Research Letters*, 41, 1752-1758,
847 10.1002/2013GL059160 (2014b)
- 848 Scinocca, J., & N. Mcfarlane (2000). The parametrization of drag induced by stratified flow over
849 anisotropic orography. *Quarterly Journal of the Royal Meteorological Society*, 126, 2353–
850 2394. <https://doi.org/10.1256/smsqj.56801>
- 851 Smith, R., Jones P., Briegleb B., Bryan F., Danabasoglu G., Dennis J., et al. (2010). The Parallel
852 Ocean Program (POP) reference manual, Ocean component of the Community Climate
853 System Model (CCSM), *LANL Technical Report*, LAUR-10-01853, 141 pp.
- 854 Sun, L., Perlitz, J., Richter, J. H., Hoerling, M. P., & Hurrell, J. W. (2020). Attribution of NAO
855 predictive skill beyond 2 weeks in boreal winter. *Geophysical Research Letters*, 47,
856 e2020GL090451. <https://doi.org/10.1029/2020GL090451>
- 857 Stan C., Straus, D. M., Frederiksen, J. S., Lin, H., Maloney, E. D., & Schumacher, C., et al.
858 (2017). Review of Tropical-Extratropical Teleconnections on Intraseasonal Time Scales.
859 *Review of Geophysics*, 55, 902-937.
- 860 Tolman, H. L. (2009). User manual and system documentation of WAVEWATCH III TM
861 version 3.14. *Technical note, MMAB Contribution*, 276, p.220.
- 862 Tripathi, O. P., Baldwin, M., Charlton-Perez, A., Charron, M., Eckermann, S.D., Gerber, E., et
863 al. (2015). The predictability of the extratropical stratosphere on monthly time-scales and its
864 impact on the skill of tropospheric forecasts. *Quarterly Journal of the Royal Meteorological
865 Society*, 141: 987-1003. <https://doi.org/10.1002/qj.2432>
- 866 Tsujino, H., Urakawa S., Nakano H., Small R. J., Kim W. M., Yeager S. G., et al. (2018). JRA-
867 55 based surface dataset for driving ocean–sea-ice models (JRA55-do). *Ocean Modelling*,
868 130, 79–139, <https://doi.org/10.1016/j.ocemod.2018.07.002>.

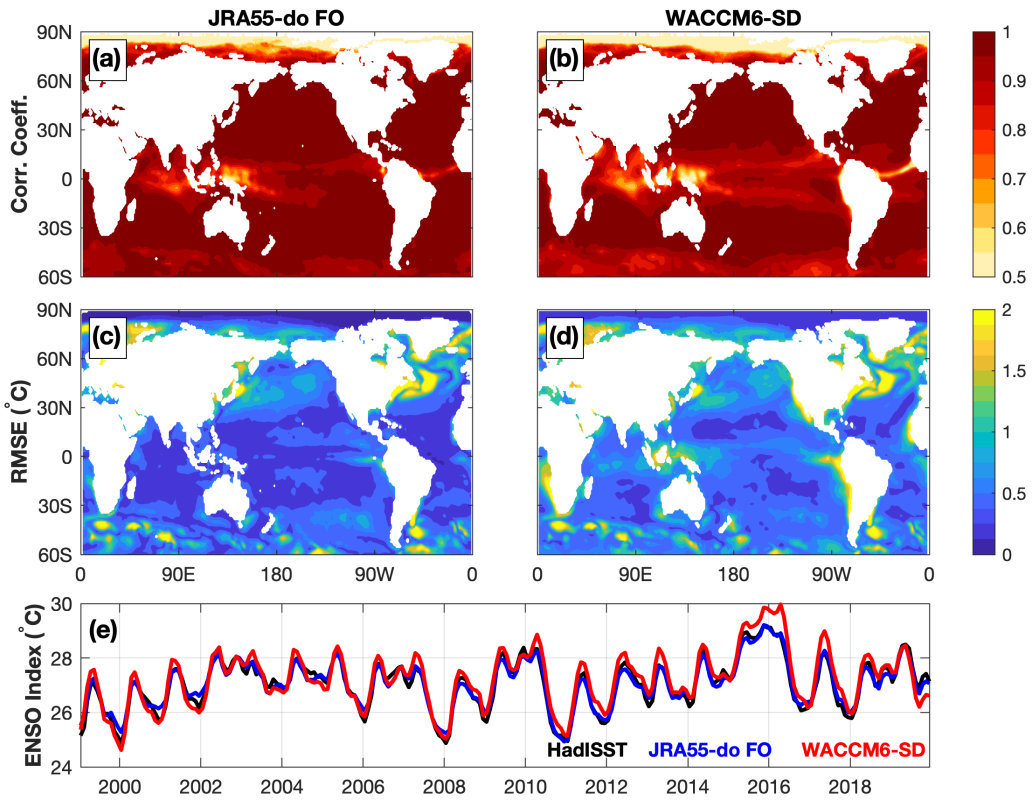
- 869 Tsujino, H., Urakawa L. S., Griffies S. M., Danabasoglu G., Adcroft A. J., Amaral A. E., et al.
870 (2020). Evaluation of global ocean–sea-ice model simulations based on the experimental
871 protocols of the Ocean Model Intercomparison Project phase 2 (OMIP-2). *Geoscience Model
872 Development*, 13, 3643–3708, <https://doi.org/10.5194/gmd-13-3643-2020>.
- 873 Vitart, F., C. Ardilouze, A. Bounet, A. Brookshaw, M. Chen, C. Codorean, et al. (2017). The
874 Subseasonal to Seasonal (S2S) Prediction Project Database. *Bulletin of the American
875 Meteorological Society*, 98, 163–173. doi:10.1175/BAMS-D-16-0017.1.
- 876 Vitart, F. (2017). Madden–Julian Oscillation prediction and teleconnections in the S2S database.
877 *Quarterly Journal of the Royal Meteorological Society*, 143, 2210–2220.
878 <https://doi.org/10.1002/qj.3079>
- 879 Vitart, F., & A. W. Robertson (2018). The sub-seasonal to seasonal prediction project (S2S) and
880 the prediction of extreme events. *npj Climate Atmospheric Science*, 1, 3,
881 <https://doi.org/10.1038/S41612-018-0013-0>.
- 882 Wang H., Akmaev, R. A., Fang, T.-W., Fuller-Rowell, T. J., Wu, F., Maruyama, N., & Iredell,
883 M. D. (2014). First forecast of a sudden stratospheric warming with a coupled whole-
884 atmosphere/ionosphere model IDEA, *Journal of Geophysical Research: Space Physics*, 119,
885 2079–2089, doi:10.1002/2013JA019481.
- 886 Wang, L., & Robertson, A. W. (2019). Week 3–4 predictability over the United States assessed
887 from two operational ensemble prediction systems. *Climate Dynamics*, 52(9-10), 5861–5875.
888 <https://doi.org/10.1007/s00382-018-4484-9>.
- 889 Wayand, N. E., Bitz, C. M., & Blanchard-Wrigglesworth, E. (2019). A year-round subseasonal-
890 to-seasonal sea ice prediction portal. *Geophysical Research Letters*, 46, 3298–3307.
891 <https://doi.org/10.1029/2018GL081565>

- 892 White, C. J., and Carlsen H., Robertson A. W., Klein R. J. T., Lazo J. K., Kumar A., et al.
893 (2017). Potential applications of Subseasonal-to-Seasonal (S2S) predictions. *Meteorological*
894 *Applications*, 24, 315–325, <https://doi.org/10.1002/met.1654>.
- 895 Wilks, D. S. (2011). Statistical Methods in the Atmospheric Sciences. 3rd ed. International
896 Geophysics Series, Vol. 100, Academic Press, 704 pp.
- 897 Xiang, B., Sun, Y. Q., Chen, J.-H., Johnson, N. C., & Jiang, X. (2020). Subseasonal prediction of
898 land cold extremes in boreal wintertime. *Journal of Geophysical Research: Atmospheres*,
899 124, e2020JD032670. <https://doi.org/10.1029/2020JD032670>
- 900 Yamagami, A., & Matsueda, M. (2020). Subseasonal forecast skill for weekly mean atmospheric
901 variability over the Northern Hemisphere in winter and its relationship to midlatitude
902 teleconnections. *Geophysical Research Letters*, 47, e2020GL088508. <https://doi.org/10.1029/2020GL088508>
- 903 Zampieri, L., Goessling, H. F., & Jung, T. (2018). Bright prospects for Arctic Sea ice prediction
904 on subseasonal time scales. *Geophysical Research Letters*, 45, 9731–9738.
905 <https://doi.org/10.1029/2018GL079394>
- 906 Zar, J.H., (2014). Spearman Rank Correlation: Overview. Wiley StatsRef: Statistics Reference
907 Online. doi:10.1002/9781118445112.stat05964
- 909 Zhang, G. J., & McFarlane, N. A. (1995). Sensitivity of climate simulations to the
910 parameterization of cumulus convection in the Canadian Climate Center general circulation
911 model. *Atmosphere-Ocean*, 33, 407–446.
- 912 Zuo J., H-L. Ren, J. Wu, Y. Nie, Q. Li (2016). Subseasonal variability and predictability of the
913 Arctic Oscillation/North Atlantic Oscillation in BCC_AGCM2.2, Dynamics of Atmospheres
914 and Oceans, 75, pp 33-45, <https://doi.org/10.1016/j.dynatmoce.2016.05.002>

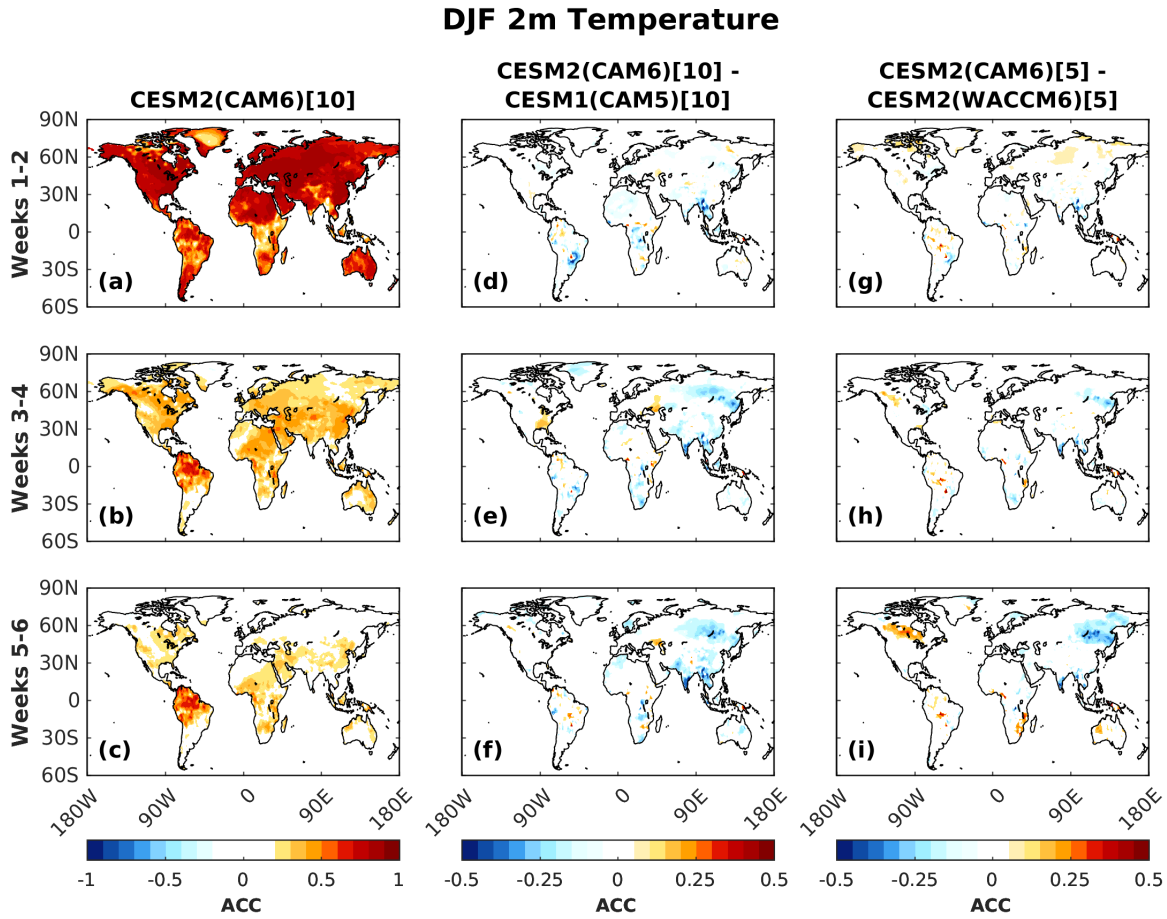
916

917

918

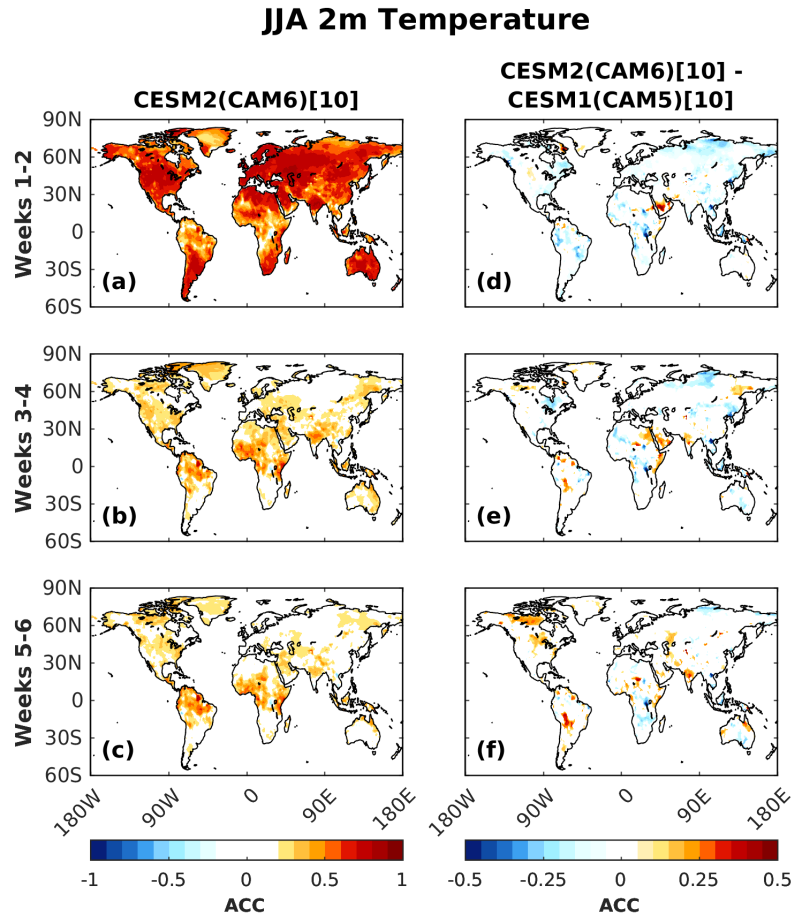
919
920

921 **Figure 1:** Correlation coefficients for SST from (a) JRA55-do FO (b) WACCM6-SD in
 922 comparison with HadISST observations. RMSE for (c) JRA55-do FO and (d) WACCM6-SD
 923 when compared with the same observations. (e) The ENSO Nino3.4 Index (e) for all the datasets.
 924 All calculations use monthly data from 1999-2019.
 925



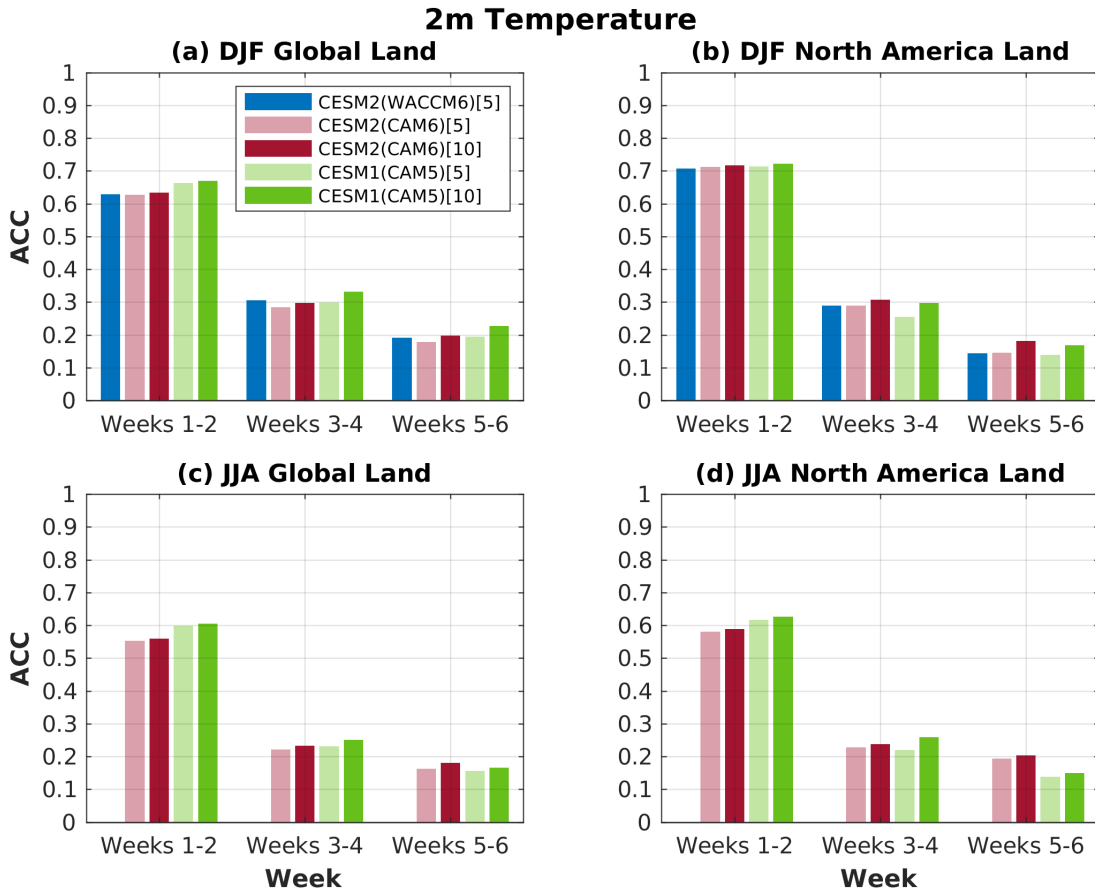
926
927
928
929
930
931
932
933
934
935
936
937

Figure 2: The DJF 2m temperature ACC for CESM2(CAM6) over land for (a) weeks 1-2 (day 1-14 averaged), (b) weeks 3-4 (day 15-28 averaged), and (c) weeks 5-6 (day 29-42 averaged). Using the same biweekly separation, panels (d)-(f) show the difference in ACC for CESM2(CAM6) minus CESM1(CAM5) and panels (g)-(i) show the difference in ACC for CESM2(CAM6) minus CESM2(WACCM6). Data in the difference plots that fall below the 95% confidence level using a Fisher z transformation are omitted. Note the different colorbar ranges. All calculations use daily data from 1999-2015. The number of ensemble members used in the analysis is given in the column titles in the square brackets.



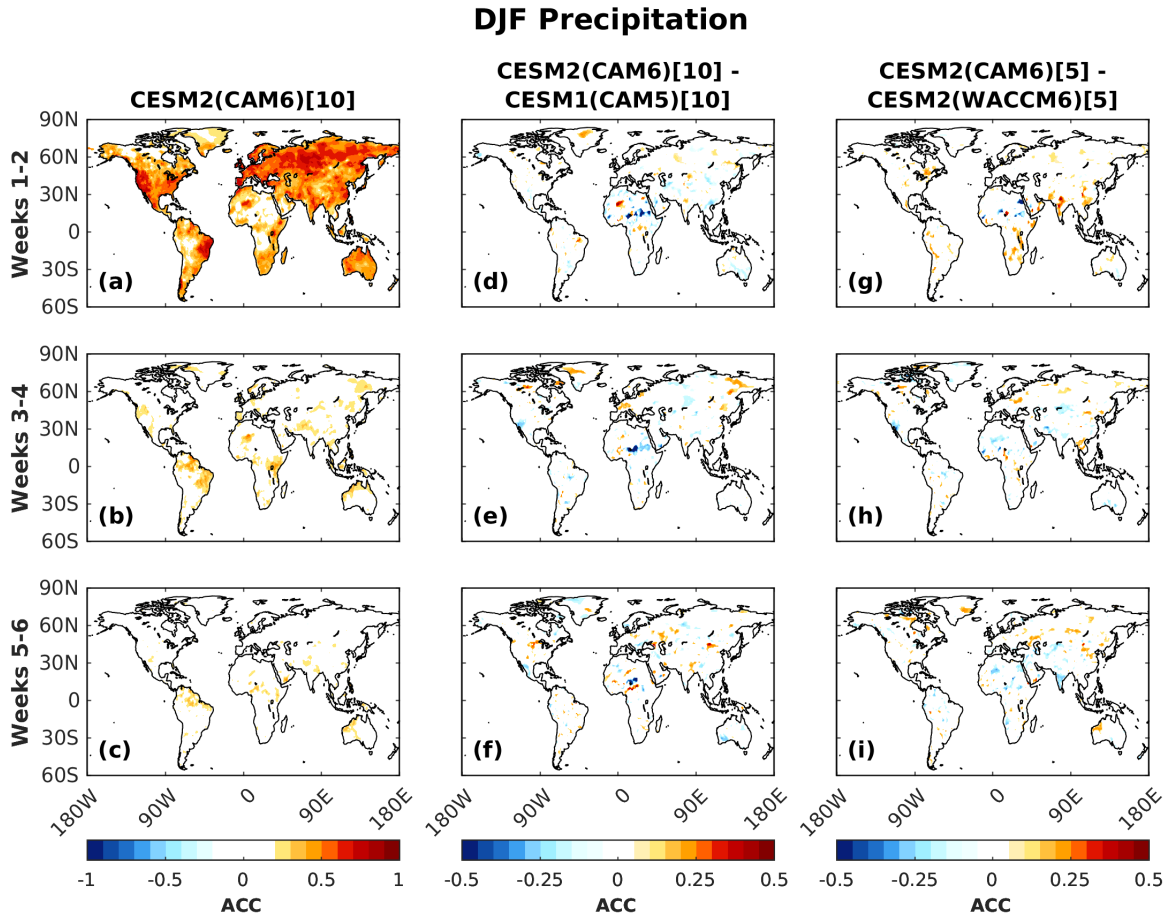
938
939

940 **Figure 3:** Same as Figure 2 but for JJA. Note, there is no CESM2(WACCM6) data for April -
941 August.
942
943
944
945
946
947
948
949
950
951
952



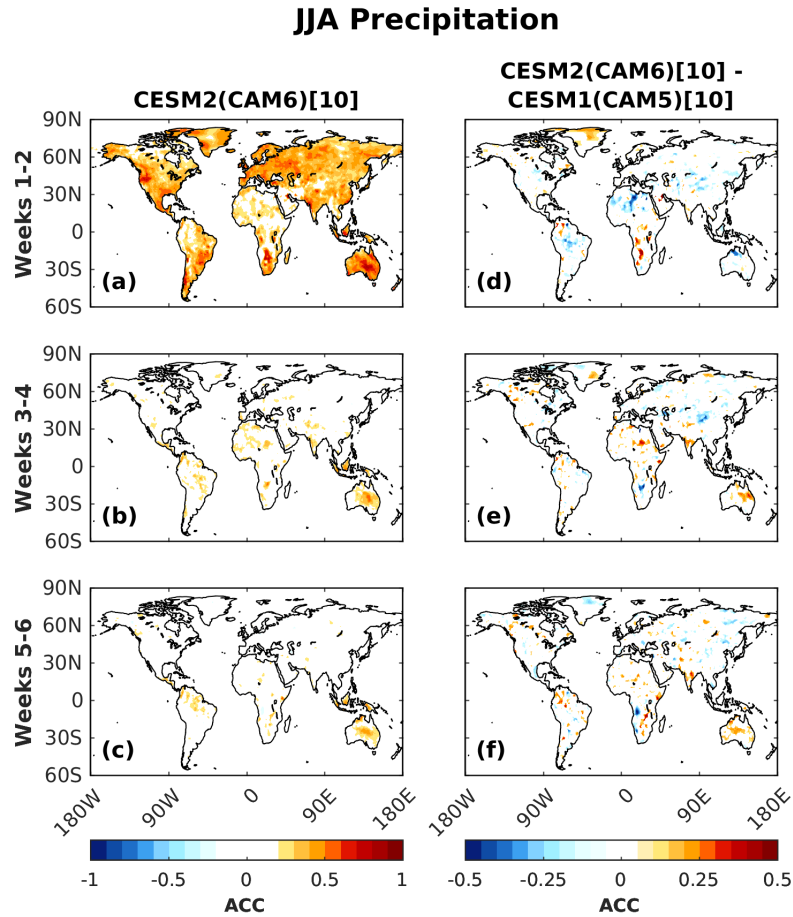
953
954
955
956
957
958
959
960
961
962
963
964

Figure 4: DJF 2m temperature ACC averaged over (a) the global land and (b) North American land. Panels (c) and (d) are the same as panels (a) and (b) but for JJA. Note, there is no CESM2(WACCM6) data for April - August. All calculations use daily data from 1999-2015. In the legend, the number of ensemble members used in the calculations is shown in square brackets.



965
966
967
968

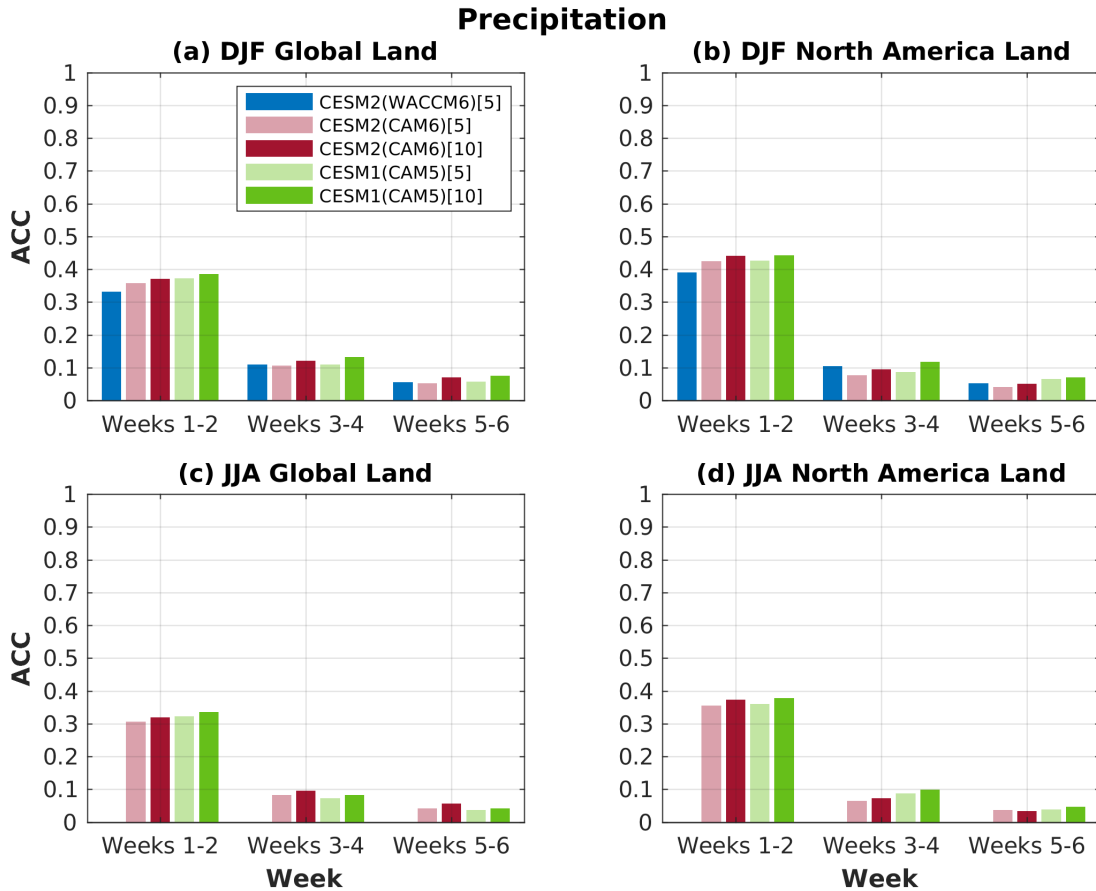
Figure 5: Same as Figure 2 but for precipitation.



969
970

971 **Figure 6:** Same as Figure 3 but for precipitation.

972
973



974
975
976 **Figure 7:** Same as Figure 4 but for precipitation.
977
978
979
980

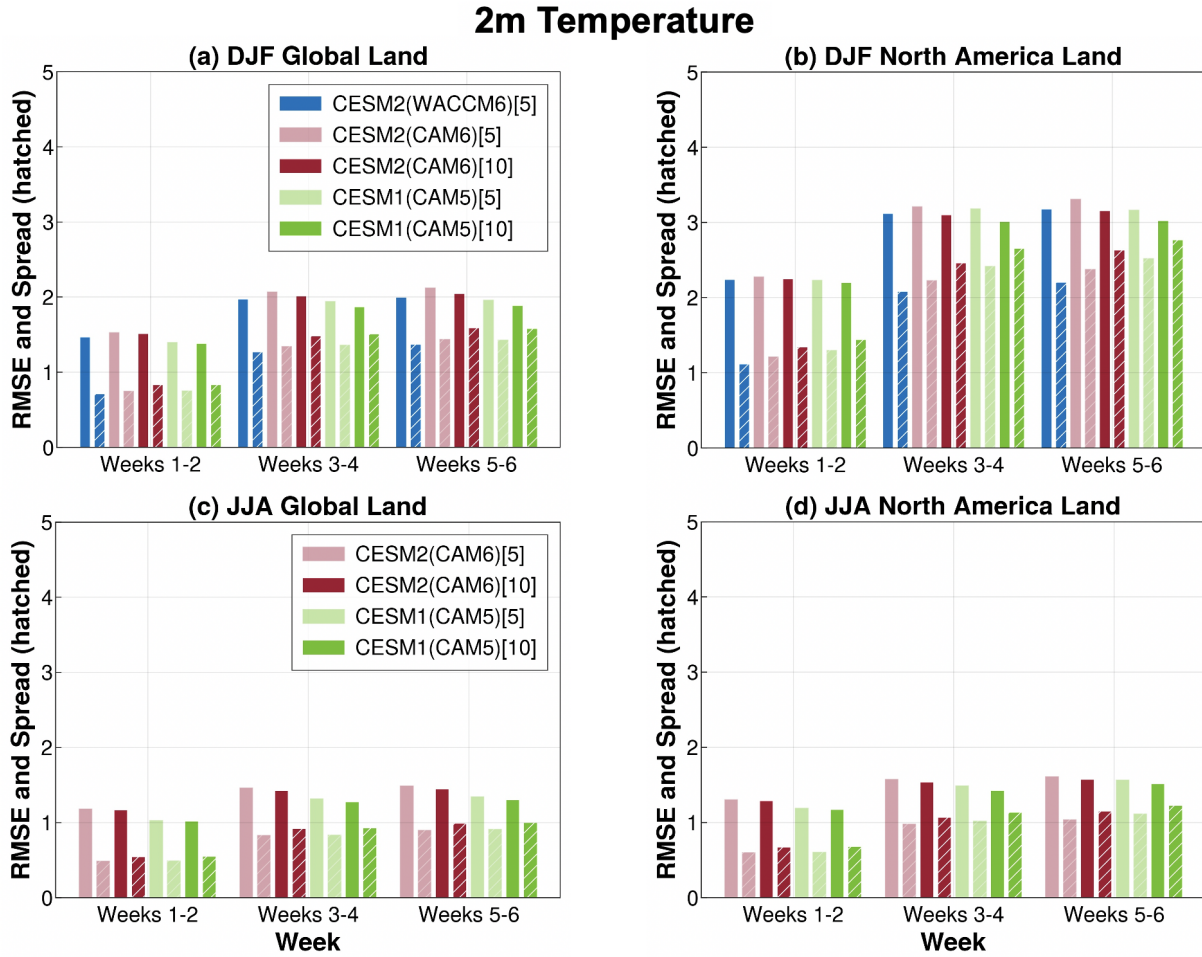
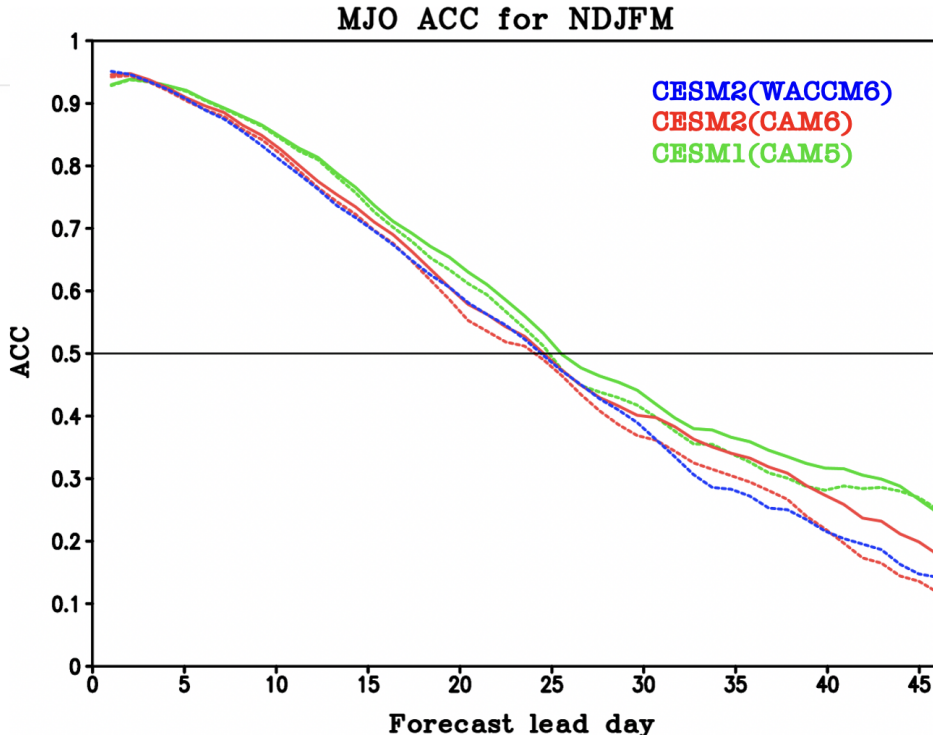
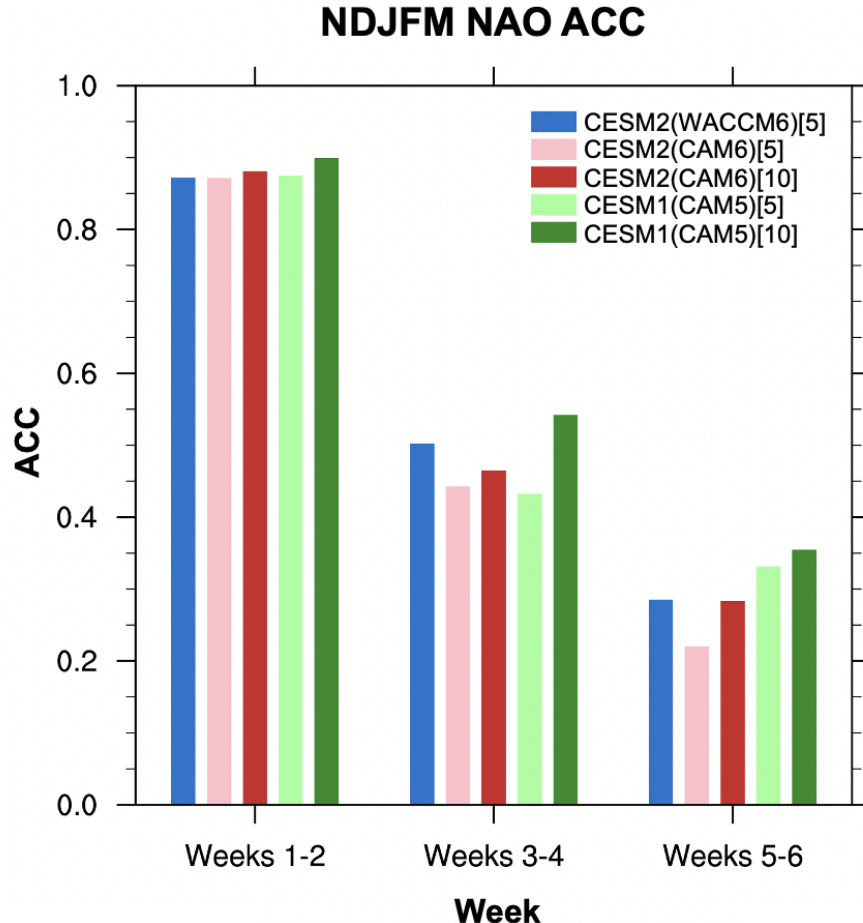


Figure 8. RMSE (solid bars) and spread (hatched bars) for 2m temperature for DJF (top) and JJA (bottom). Metrics are shown for global land (left) and North American land (right).

981
982
983
984
985
986
987
988
989



990
991
992 **Figure 9:** ACC for MJO for NDJFM from CESM1(CAM5), CESM2(CAM6), and
993 CESM2(WACCM6). Solid (dashed) lines indicate the average of 10 (5) ensemble members.
994
995



996
997 **Figure 10:** Biweekly NAO ACC in NDJFM from CESM1(CAM5), CESM2(CAM6), and
998 CESM2(WACCM6). The number of ensemble members used in the analysis is given in the
999 square brackets.

1000
1001
1002
1003
1004
1005
1006

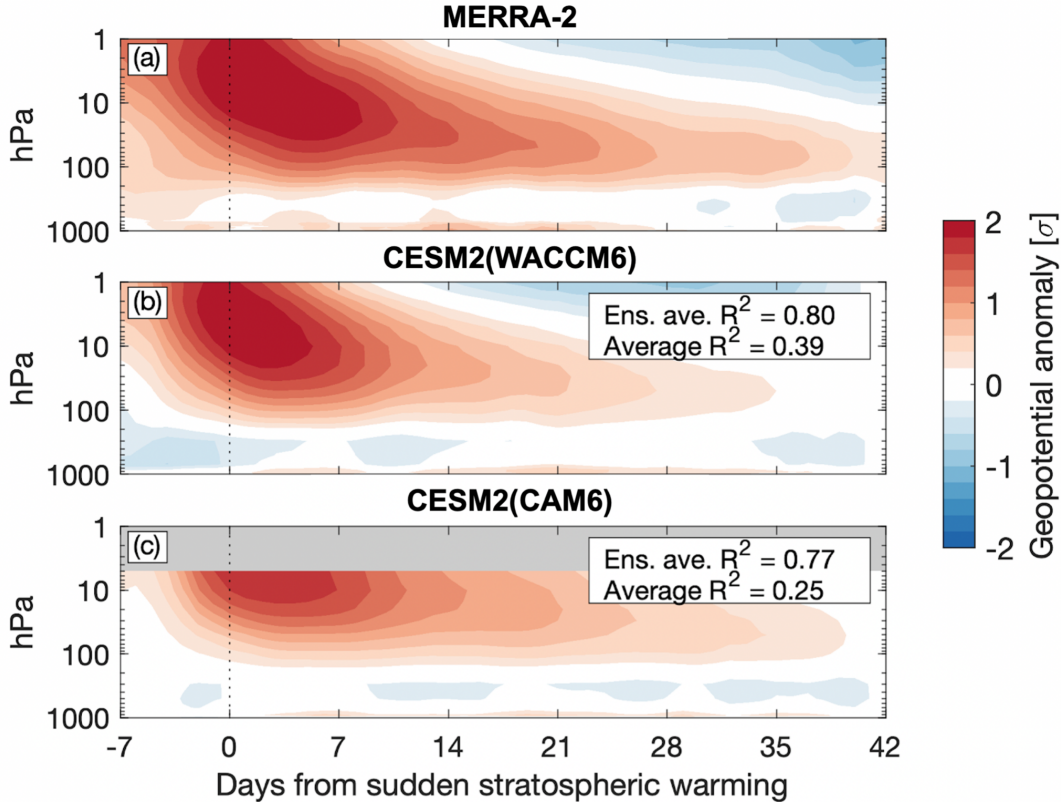
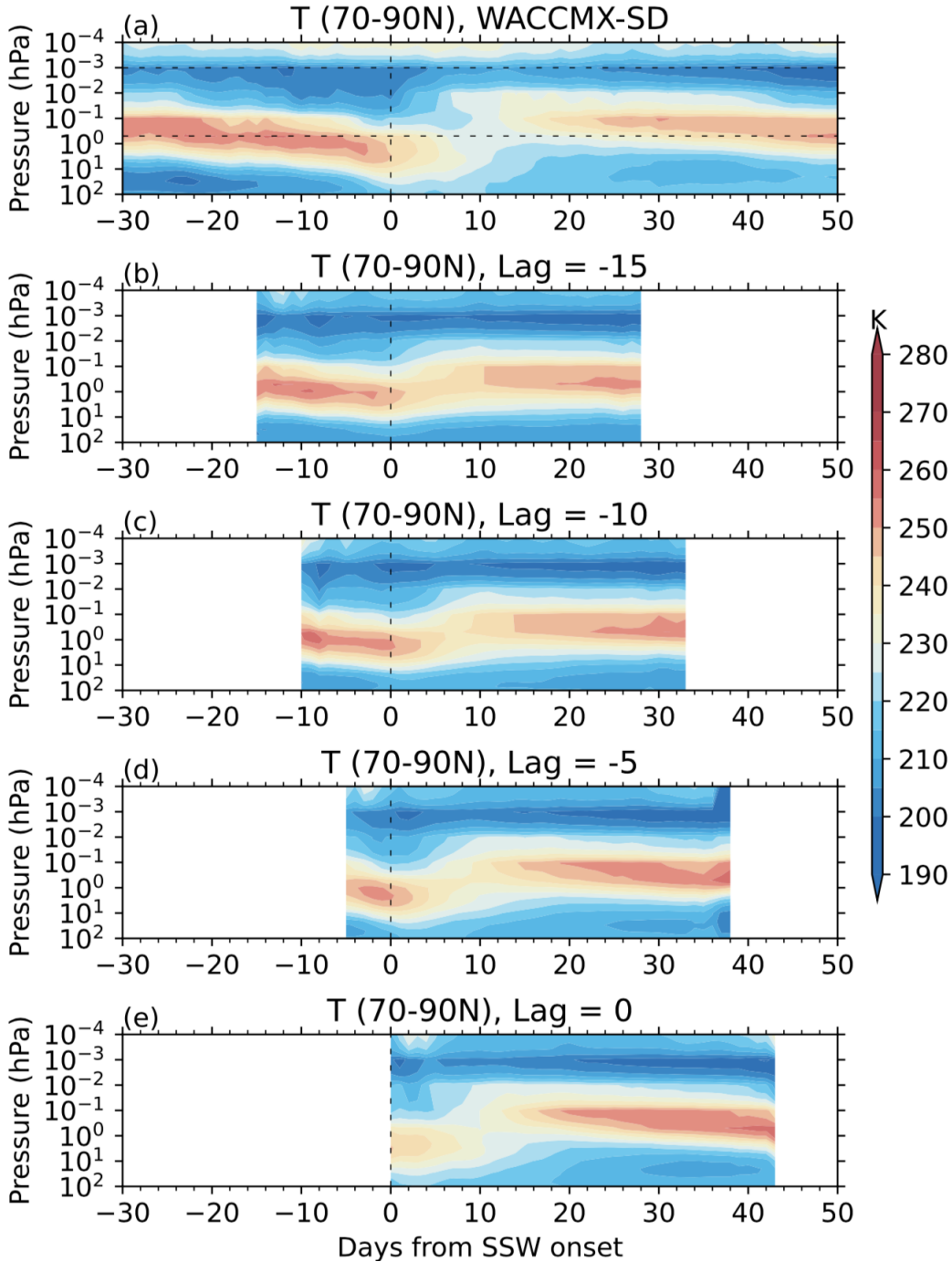


Figure 11: Standardized polar cap geopotential anomalies composited around the central SSW date for (a) MERRA-2, (b) CESM2(WACCM6) reforecasts, and (c) CESM2 reforecasts, shaded every 0.2 standard deviations. The squared pattern correlation between the ensemble average of the reforecasts and MERRA-2, as well as the average of all squared correlations between each individual ensemble member and MERRA-2 for every event, are displayed in the upper right of each panel.

1007
1008
1009
1010
1011
1012
1013
1014
1015



1016
1017
1018
1019
1020
1021
1022
1023
1024

Figure 12: Composite of zonal-mean temperature (T) between 70°-90°N for 14 major SSW events in (a) WACCMX-SD, and CESM2(WACCM6) reforecasts initialized at a lag of (b) -15, (c) -10, (d) -5, and (e) 0 days prior to the SSW central date. The SSW onset date is defined as the zonal-mean zonal wind reversal at 60N and 10 hPa. The horizontal dashed lines in panel (a) mark the stratopause (~ 0.5 hPa), and mesopause ($\sim 10^{-3}$ hPa respectively).

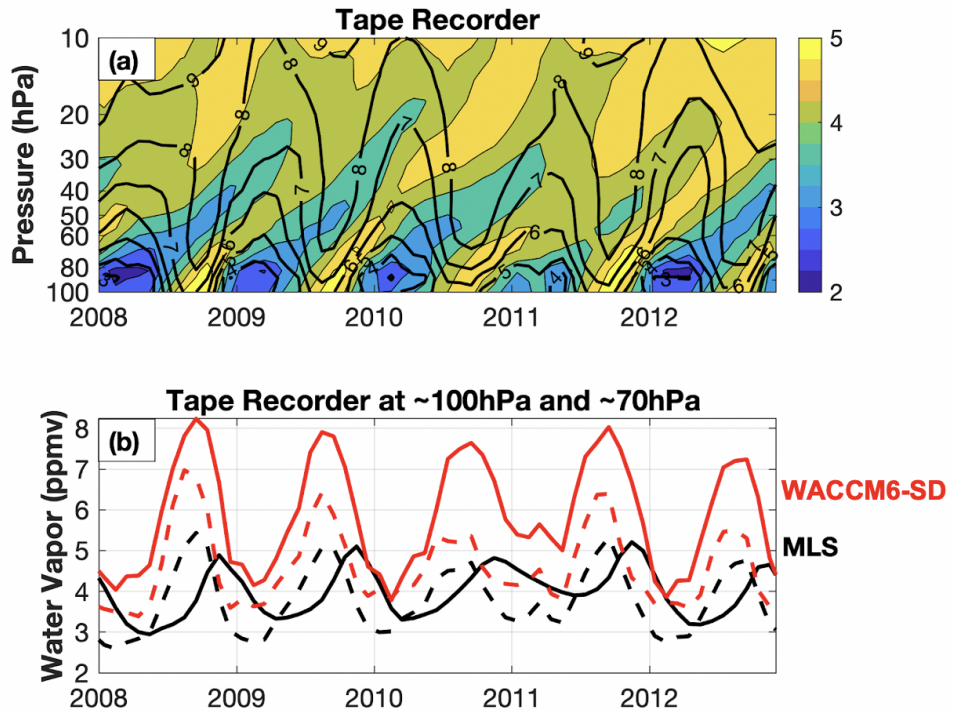


Fig 14: The 10°S - 10°N tape recorder of water vapor (a) for MLS observations (filled color contours) and WACCM6-SD (back contour lines). The time series of the tape recorder at $\sim 100\text{hPa}$ (dashed lines) and $\sim 70\text{hPa}$ (solid lines) for MLS (black) and WACCM6-SD (red).

1025
1026
1027
1028
1029
1030
1031
1032
1033
1034

1035
1036

	Atmosphere	Land	Ocean & Sea-ice	Reforecast Period	Initialization Frequency	# Ens Members Rforecasts	# Ens Members Forecasts
CESM2 (CAM6)	CFSv2	CLM5 spun up with CFSv2	JRA55-do forced ocn/sea-ice	All months, 1999 - 2020	Every Monday*	11	21**
CESM2 (WACCM6)	WACCM6-SD run nudged to MERRA-2	CLM5 spun up with CFSv2	Hybrid: JRA55-do every 5 yrs / MERRA-2 forced ocn	Sep-Mar 1999 - 2020	Every Monday*	5	21***

1037

1038

1039

1040

1041

1042

1043

1044

Table 1: Summary of initialization methods for S2S reforecasts with CESM2(CAM6) and CESM2(WACCM6). *Reforecasts are started every Monday, except for leap years, in which case the reforecast was carried out on a Sunday; **Real-time forecasts with CESM2(CAM6) stared April 2021; *** Real-time forecasts with CESM2(WACCM6) started in September 2020.